Theoretical Biophysics
A Computational Approach
Concepts, Models, Methods and Algorithms
Membranes

Dieter W. Heermann

April 7, 2020

Heidelberg University

Table of Contents

Introduction

Introduction I

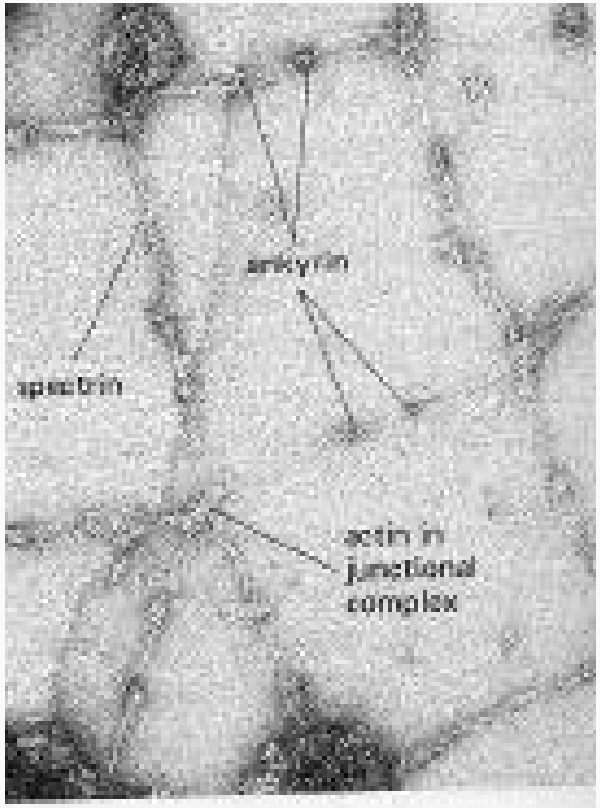

Figure 1: An example of a two-dimensional network in a cell taken from [1]. This figure shows an example of a two-dimensional network in a cell. Shown is the membrane-associated cytoskeleton of the human erythrocyte. The image showes that there is a network of spectrin tetramers attached to cytoplasmic side of plasma membrane about midway along their length by the protein ankyrin. Each spectrin tetramer has a 200 *nm* contour length with an end-to-end distance of $< R_e > \ 70\ nm$.

Introduction II

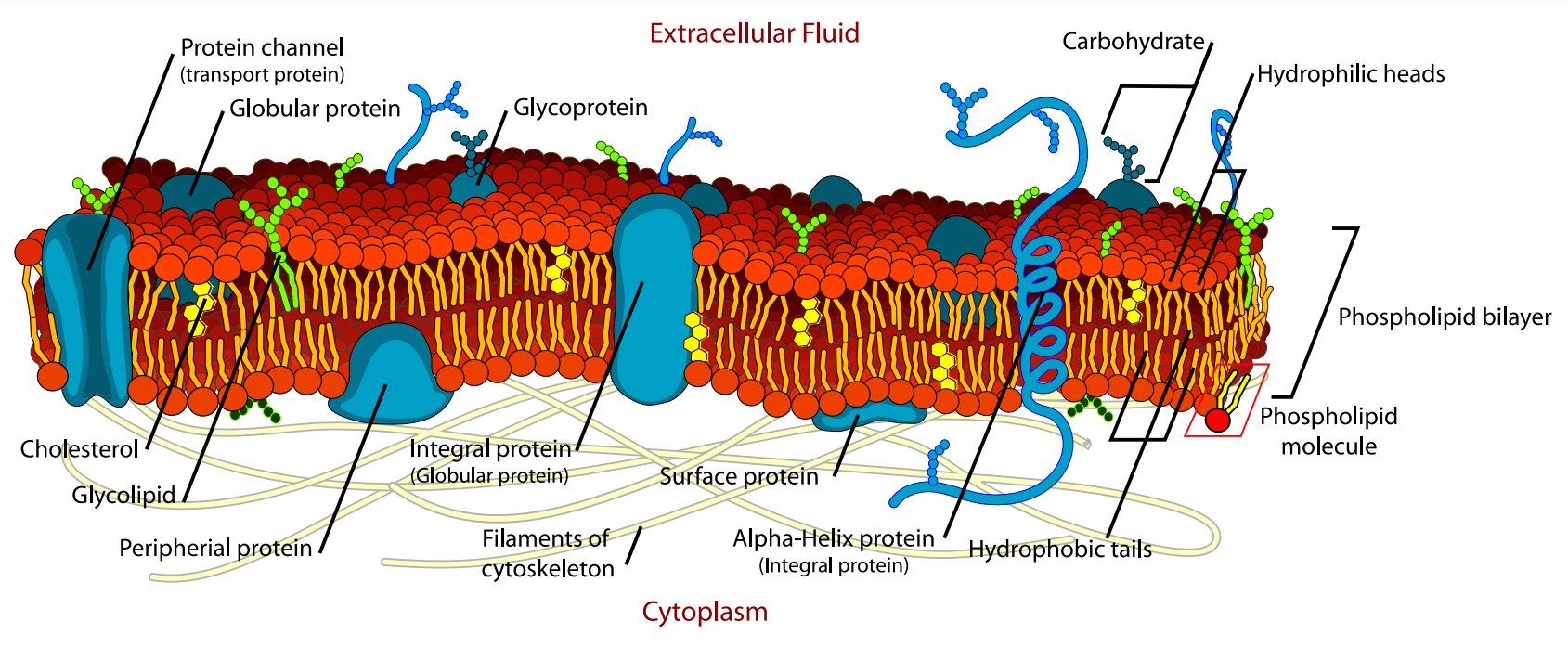

Figure 2: Image taken from wikipedia (https://en.wikipedia.org/wiki/Membrane_models).

Introduction III

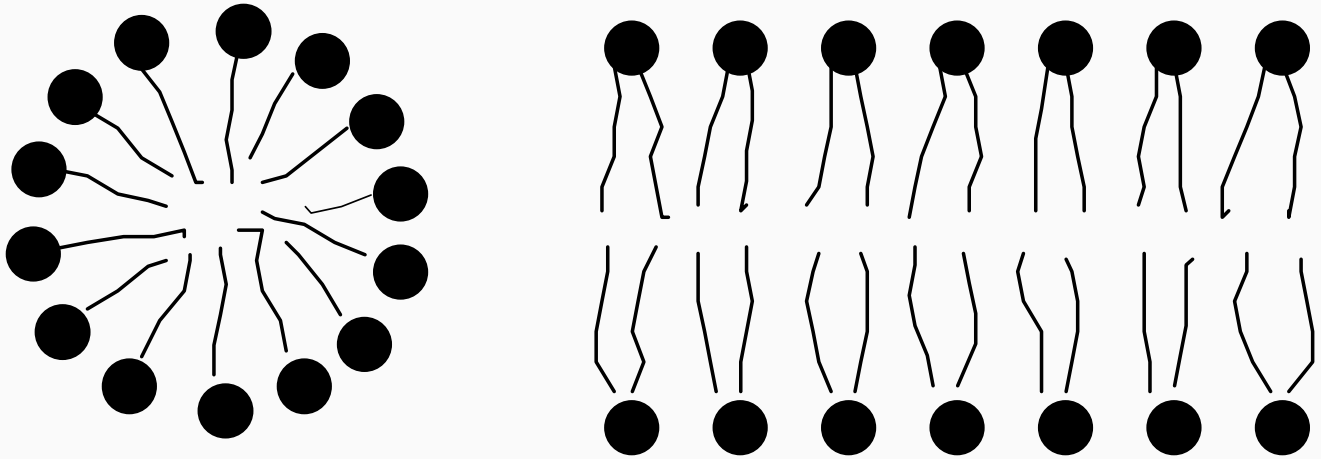

Figure 3: A micell and a lipid bi-layer model.

Introduction IV

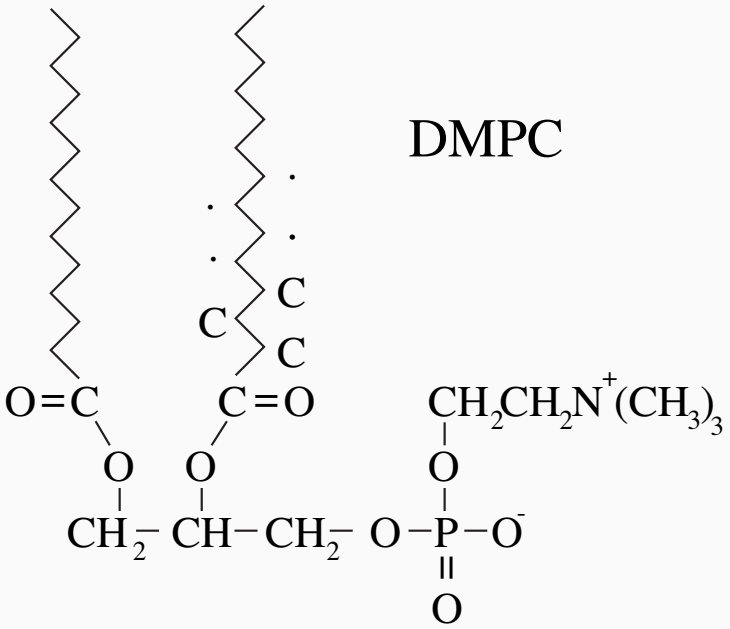

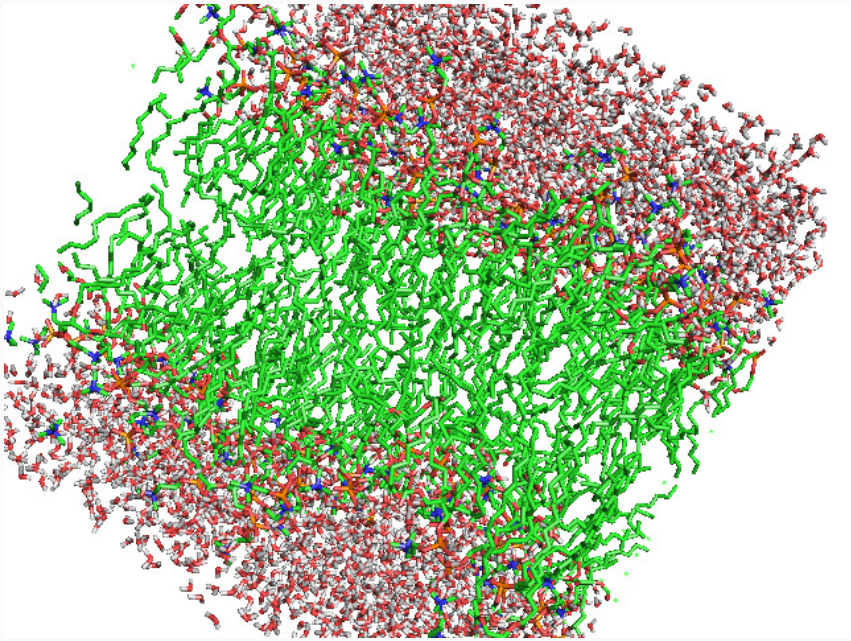

Figure 4: The figure shows 128 DMPC lipids and 3655 water molecules. 1 ns of constant area at $0.596 nm^2$. Downloaded and taken from Peter Tielemans website http://www.ucalgary.ca/ tieleman/download.html.

Introduction V

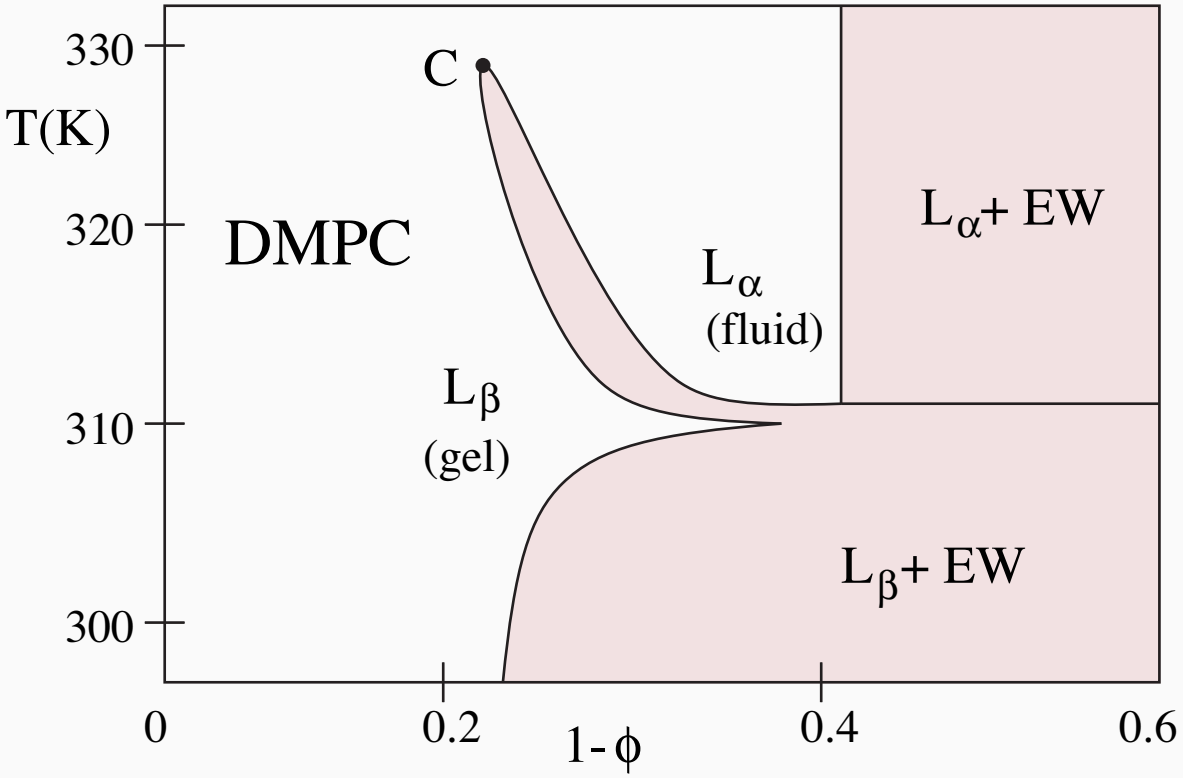

Figure 5: Phase diagram for the DMPC as a function of lipid volume fraction ϕ. Downloaded and taken from Peter Tielemans website http://www.ucalgary.ca/ tieleman/download.html.

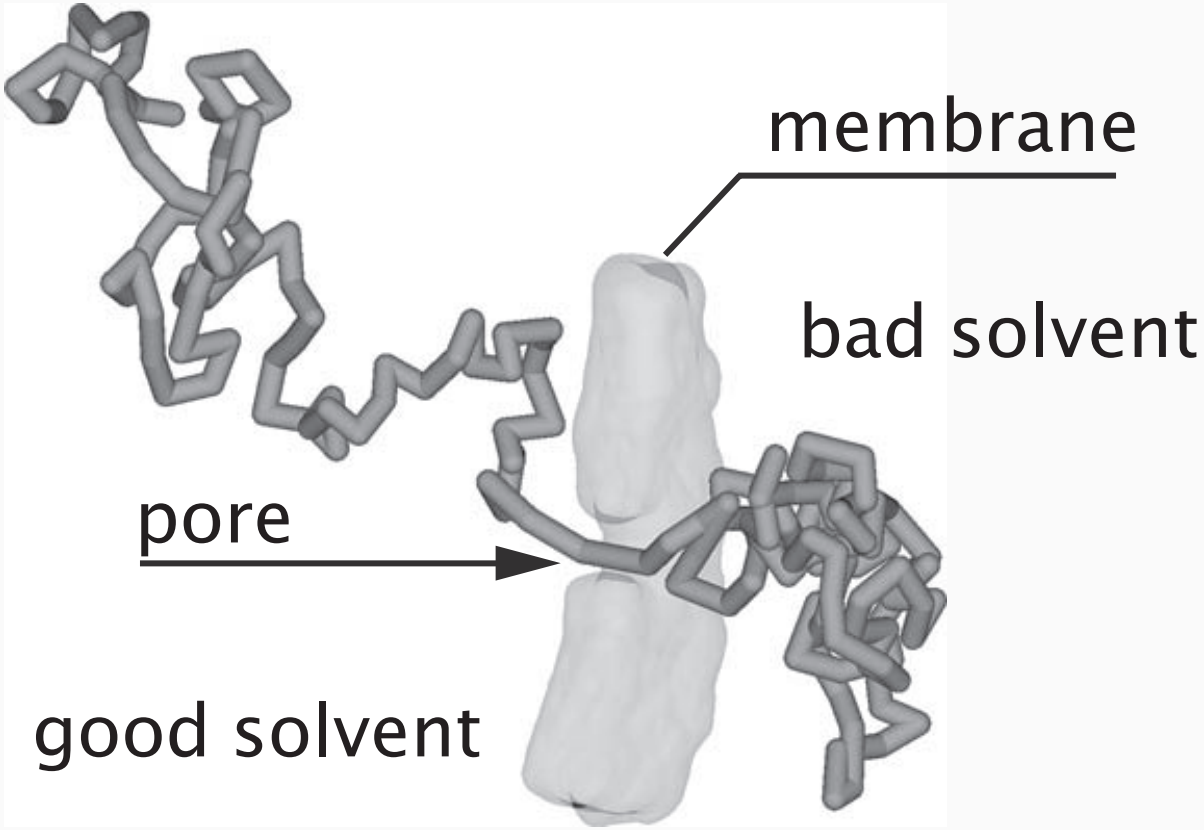

Figure 6: Translocation of a macromolecule through a membrane pore. Image taken from [2]

Introduction VII

Possible membrane models include:

- fixed triangulation
- dynamic triangulation (liquid membranes)
- all-atom model
- coarse-grained polymer models
- lattice models with placettes
- lattice Potts-model-like

Differential geometry of surfaces I

- We shall first be concerned with the intrinsic and extrinsic geometric properties of surfaces, such as the curvature.
- For simplicity we consider a surface S which is the graph of a function with continuous second derivatives.
- This may be of the form $z = f(x, y)$ or parameterized $f(s, t), g(s, t), h(s, t)$ for a two-dimensional surface embedded in three-dimensional space.
- Let **n** denote a unit normal vector to S at a point **p** choosen such that the normal vector is pointing along the z-axis.
- Now slice S by planes containing **n** and consider the curvature of the resulting curves.
- The curvatures of these resulting curves are called **normal curvatures** at **p**.
- The maximum normal curvature κ_1 and the minimum normal curvature κ_2 are called **principal curvatures**.
- The **Gaussian curvature** $K(\mathbf{p})$ at any point p on S is the product of the extreme curvatures of the curves through **p** cut out by normal planes (the product of the principal curvatures).

- The Gaussian curvature is a measure of how much "curvedness" the surface displays. We have to be careful.
- The curvature of a curve is an extrinsic geometric property, telling how it is bent in the plane, or bent in space, whereas the Gaussian curvature is an intrinsic geometric property: it stays the same no matter how a surface is bent, as long as it is not distorted, neither stretched or compressed.
- But the mean curvature

$$H = \frac{1}{2}(\kappa_1 + \kappa_2) \tag{1}$$

  is an extrinsic property of the surface.

Let us look at the monkey saddle (see als Figure 7).

$$f(x, y) = z = x^3 - 3 * x * y^2 \ . \tag{2}$$

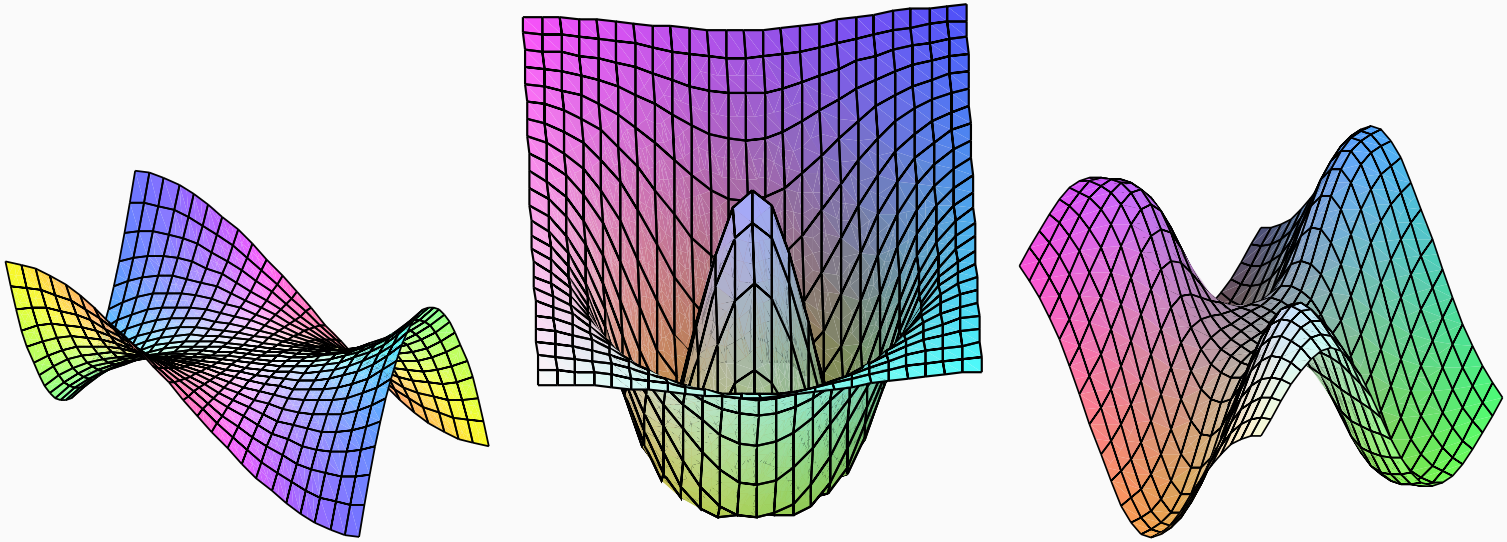

Figure 7: Shown is the monkey saddle and the corresponding curvatures.

The Gaussian curvature of the monkey saddle is given by

$$K = \frac{-36\,x^2 - 36\,y^2}{\left[1 + (3\,x^2 - 3\,y^2)^2 + 36\,x^2y^2\right]^2} \tag{3}$$

and the mean curvature by

$$H = -27\,\frac{x\left(x^4 - 2\,x^2y^2 - 3\,y^4\right)}{(1 + 9\,x^4 + 18\,x^2y^2 + 9\,y^4)^{3/2}}\ . \tag{4}$$

The energy pert unit area proposed by Helfrich on the basis of the curvature is

$$f_c = \frac{k}{2}(2H - c_0)^2 + \kappa K \tag{5}$$

where k and κ are bending rigidities and c_0 is the spontaneous curvature. Thus the free energy is

$$F = \int (f_c + \lambda) dA + \Delta p \int dV \tag{6}$$

Differential geometry of surfaces V

λ is the Lagrange multiplier for area inextensibility of the membrane, which has the same dimension as surface tension.

Membrane elasticity and bending energy I

- Fluctuating membranes and surfaces are basic structural elements of biological systems and complex fluids.
- Recent theoretical work [3, 4] and experimental studies [5, 6] indicate, that these sheetlike macromolecules should have dramatically different properties than linear polymers.
- Polymerized membranes which contain a permanently cross-linked network of constituent molecules have a shear elasticity, giving them a large entropic bending rigidity.

Membrane elasticity and bending energy II

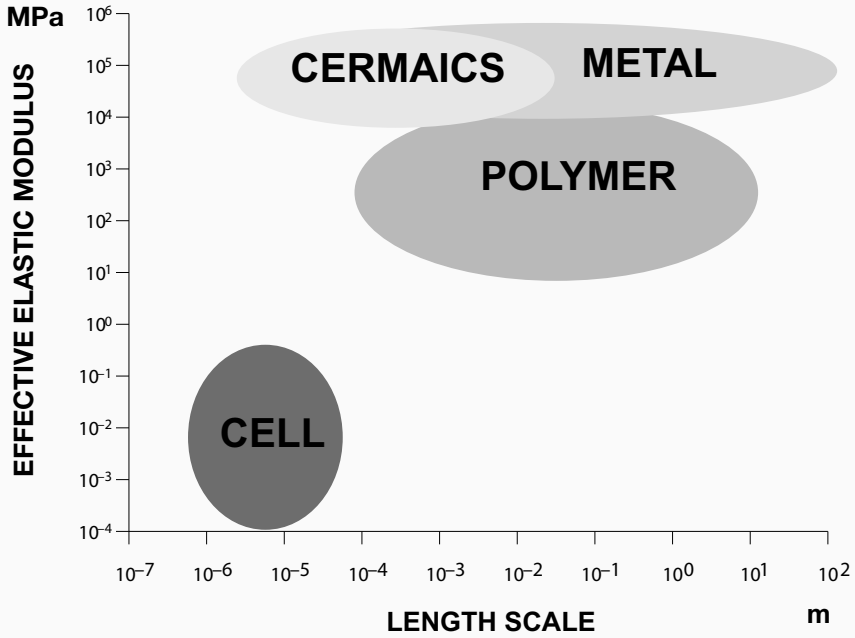

Figure 8: Comparison of the elastic modulus for different materials

- A possible approach to study the behaviour of a surface in space dimensions $D > 1$ is to discretize the surface using a triangulation [7–10].
- This, in a sense, connects with the network shown in Figure 1.

Membrane elasticity and bending energy III

- Thus the basic idea is to replace the complex network with a simple model where the edges of the triangulation represent the membrane polymers (spectrin network) and are modelled by Hookian springs with a quadratic potential.
- The surface S is thus replaced by a simplical triangulation T, specified by the number of nodes N, of links and triangles, and the X-coordinate field by the coordinates X of the nodes (see Figure 9).

Membrane elasticity and bending energy IV

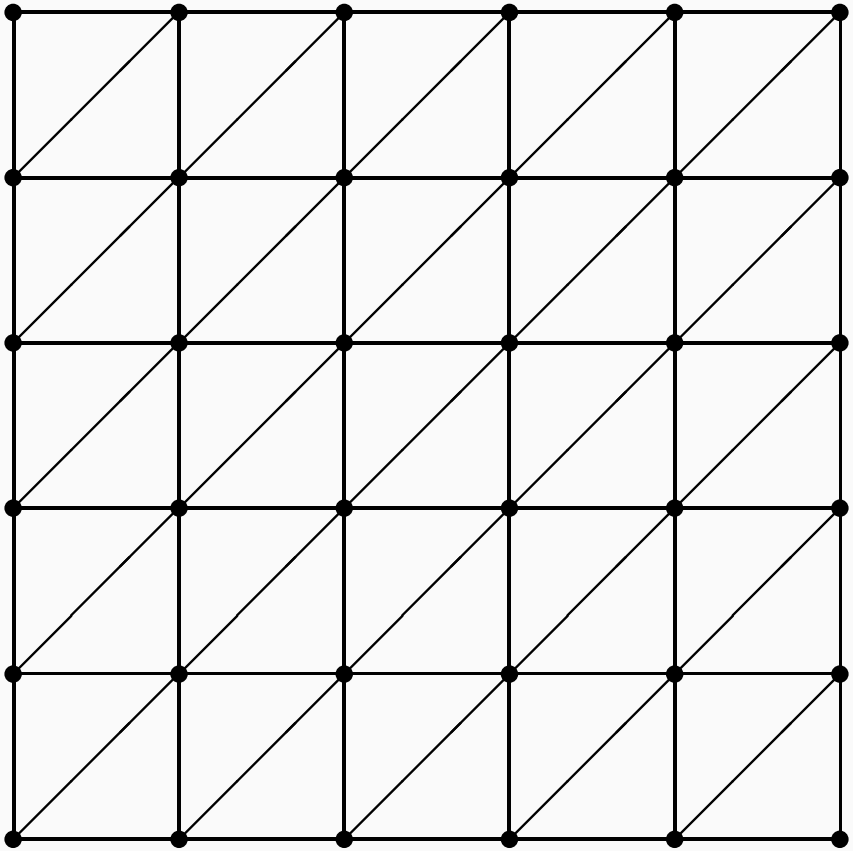

Figure 9: Triangulation model for a surface.

Membrane elasticity and bending energy V

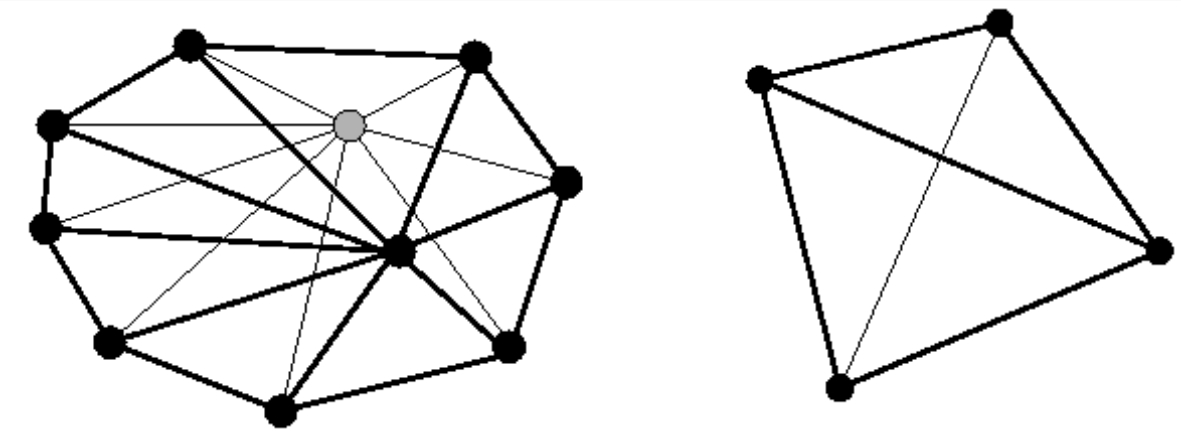

Figure 10: This figure demonstrates the elementary moves which are made for dynamically triangulated random surfaces.

- The metrical fluctuations of the manifold are modeled by summing over triangulations induced by link-flips [11–13].
- The Hamiltonian is now choosen, such that the partition function is not dominated by configurations with spikes.
- In order to suppress these spikes one adds a term with extrinsic curvature.
- As a function of the extrinsic curvature the model shows a **crumpling phase transition** at finite rigidity of the surface [14–24].

Membrane elasticity and bending energy VI

- The partition function can be written as

$$Z_N = \int d^D X_0 \int \prod_{i=1}^{N-1} d^D X_i e^{-H} \tag{7}$$

  where the translational mode is integrated out.

- The Hamiltonian H is defined as

$$H = \underbrace{\beta \cdot \sum_{\langle i,j \rangle}^{N} (X_i^\mu - X_j^\mu)^2}_{\mathcal{H}_g} + \underbrace{\lambda \cdot \sum_{\triangle_i, \triangle_j} (1 - \hat{n}_{\triangle_i} \cdot \hat{n}_{\triangle_j})}_{\mathcal{H}_e} - \underbrace{\alpha \cdot \sum_{i=0}^{N} \log \sigma_i}_{\mathcal{H}_m} \quad . \tag{8}$$

Membrane elasticity and bending energy VII

- The Gaussian part of the Hamiltonian H_g is a sum over the positions X in embedding Euclidian space of all nearest neighbours nodes, i.e. all links of the triangulation. We shall use $\beta = 1$ because of the rescaling invariance, i.e., if we rescale the coordiantes

$$X \to X' = \sqrt{\beta} X \tag{9}$$

then the partition function is replaced by

$$Z' = \beta^{(N-1)D/2} c \tag{10}$$

where c is a constant independent of β. If λ and α are both zero, then the we would obtain the average area $< A >$ as

$$< A >= -\frac{\partial \ln Z}{\partial \ln \beta} = \frac{D}{2}(N-1)\frac{1}{\beta} \tag{11}$$

and for the fluctuations

$$< A^2 > - < A >^2 = -\frac{\partial^2 \ln Z}{\partial^2 \ln \beta} = \frac{D}{2}(N-1)\frac{1}{\beta^2} \ . \tag{12}$$

Membrane elasticity and bending energy VIII

- Hence the relative width of the distribution vanishes in the thermodynamic limit

$$\lim_{N\to\infty} \frac{\sqrt{< A^2 > - < A >^2}}{< A >} = \lim_{N\to\infty} \frac{1}{\sqrt{\frac{D}{2}(N-1)}} = 0 \,. \tag{13}$$

- H_e is an *edge extrinsic curvature* term [25–32]. $\sum_{\triangle_i,\triangle_j}$ denotes a summation over all adjacent triangles which share an edge and $\hat{n}_{\triangle_i} \cdot \hat{n}_{\triangle_j}$ is the scalar product of the vectors normal to a triangle.
- The third part of the Hamiltonian H_m is the discretization of the square root of the metric. σ_i denotes the number of nearest neighbours of node i. α depends on the measure. We will set $\alpha = D/2$ for the $D = 3$ dimensional embedding space.

Membrane elasticity and bending energy IX

- We expect that the above model shows a phase transition at some critical value of the coupling λ. There are several questions which we want to address: What is the order of the transition?
- If the transition is of second order, what are the exponents?
- Are the exponents topology dependent?
- Is the transition temperature topology dependent?
- We want to look at the closed dynamically triangulated random surfaces without self-avoidance.
- As models for such surfaces we take the first two topologically closed surfaces:
  - The sphere and the torus (c.f. Figure 11).
  - The torus is specified by identifying edges of the parameter space $\mathcal{P}$.

Membrane elasticity and bending energy X

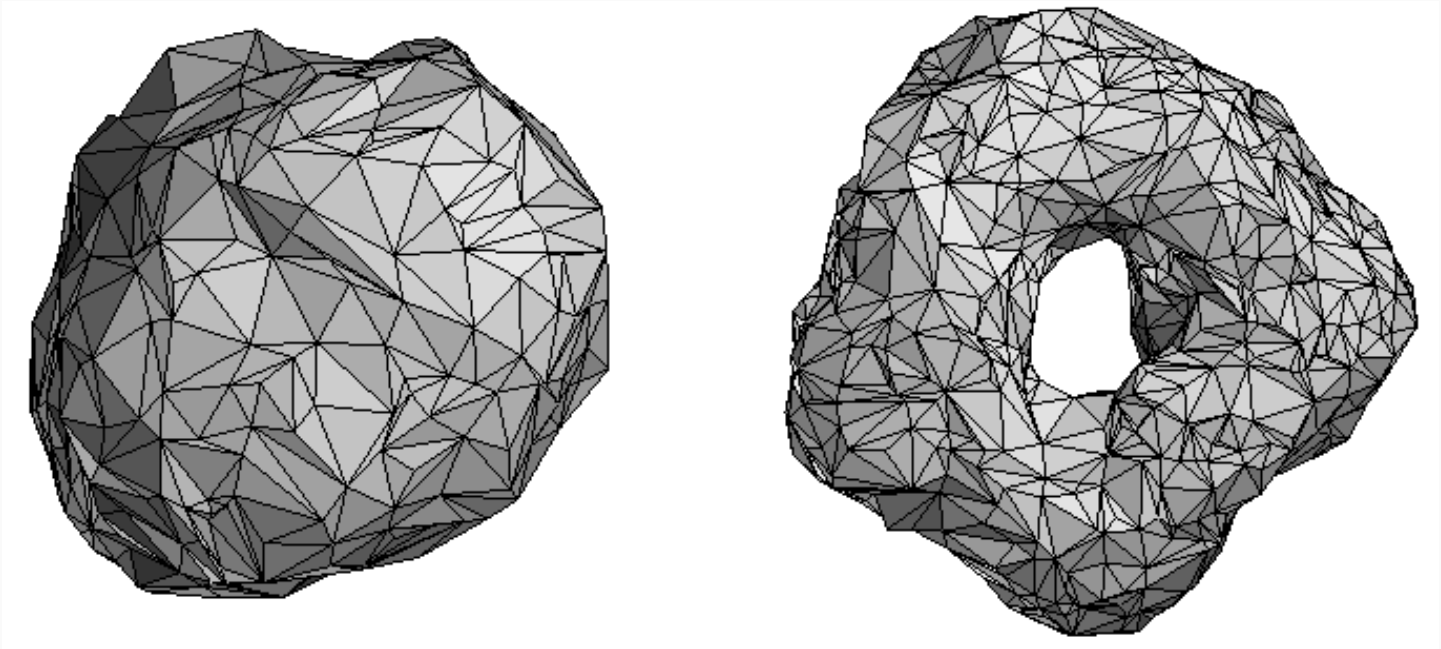

Figure 11: *Shown are two examples of configurations of dynamically triangulated random surfaces. The left picture shows a sphere and the right part a torus.*

UNIVERSITÄT
HEIDELBERG
ZUKUNFT
SEIT 1386

Lattice Models

The Potts model [33] is a generalization of the Ising model [34] and defined as follows:

- Let $G = L^d$ be a d-dimensional lattice.
- Associated with each lattice site i is a spin s_i which can take on the values $+1$ or -1.
- The spins interact via an exchange coupling J. In addition, we allow for an external field H.
- The Hamiltonian reads

$$\mathcal{H} = -J \sum_{\langle i,j \rangle} s_i s_j + \mu H \sum_i s_i \ . \tag{14}$$

- The first sum on the right-hand side of the equation runs over nearest neighbours only.
- The symbol μ denotes the magnetic moment of a spin. If the exchange constant J is positive, the Hamiltonian is a model for ferromagnetism, i.e., the spins tend to align parallel.
- For J negative the exchange is anti ferromagnetic and the spins tend to align antiparallel. In what follows we assume a ferromagnetic interaction $J > 0$.

Membranes and Folding I

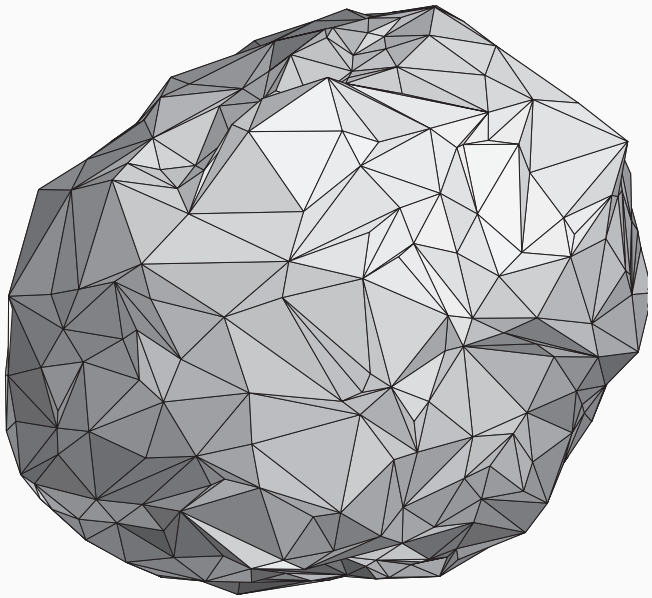

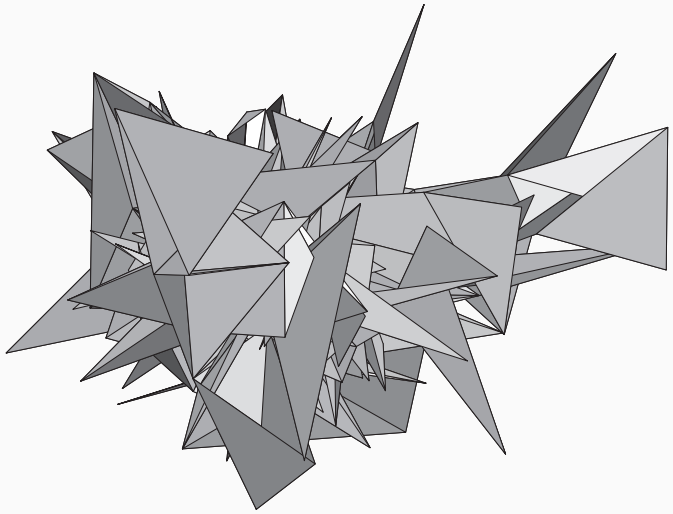

- Finite size scaling assumes, that there is only one relevant linear length scale, which is compared to the correlation length.

- To apply finite size scaling to the crumpling transition of **dynamically triangulated random surfaces** (DTRS) one must therefore assume a single length scale determined by the number of nodes N and the internal dimension d of the surface

$$L \propto N^{1/d} \quad . \tag{15}$$

- This internal dimension d also depends on the external properties of the surface and λ [35].
- So let us first look at the specific heat.
- If the transition is of second order we would have

$$C(\lambda, L) = L^{\alpha/\nu} \hat{C} \left[(\lambda - \lambda_c) L^{-\nu} \right] \tag{16}$$

where $\hat{C}$ is a scaling function, which depends on how one implements the surface.

- At the critical λ the scaling function is regular and the scaling hypotheses leads to

$$C_N^{max} \propto A N^{\alpha/\nu d} + \ldots \tag{17}$$

for the scaling of the peak in the specific heat.

- If we assume a first order transition then C_N^{max} diverges as L^d because of the δ-distribution of $C_\infty(T)$ [36–38].
- An evaluation of the specific heat C of DTRS (neglecting the metric contribution $\mathcal{H}_m$) gives the following expression

$$C_{all} = \frac{D}{2} + \frac{\lambda^2}{N}(< \mathcal{H}_e^2 > - < \mathcal{H}_e >^2) \quad . \tag{18}$$

  The first part is related to the Gaussian Hamiltonian $\mathcal{H}_g$ and the second to the specific heat C of the edge extrinsic curvature $\mathcal{H}_e$.
- The specific heat for the edge extrinsic curvature is shown in Figure 12 for the two topologies considered.
- The interpolation was done by the method of Ferrenberg and Swendsen [39, 40] using histograms of $\mathcal{H}_e$.

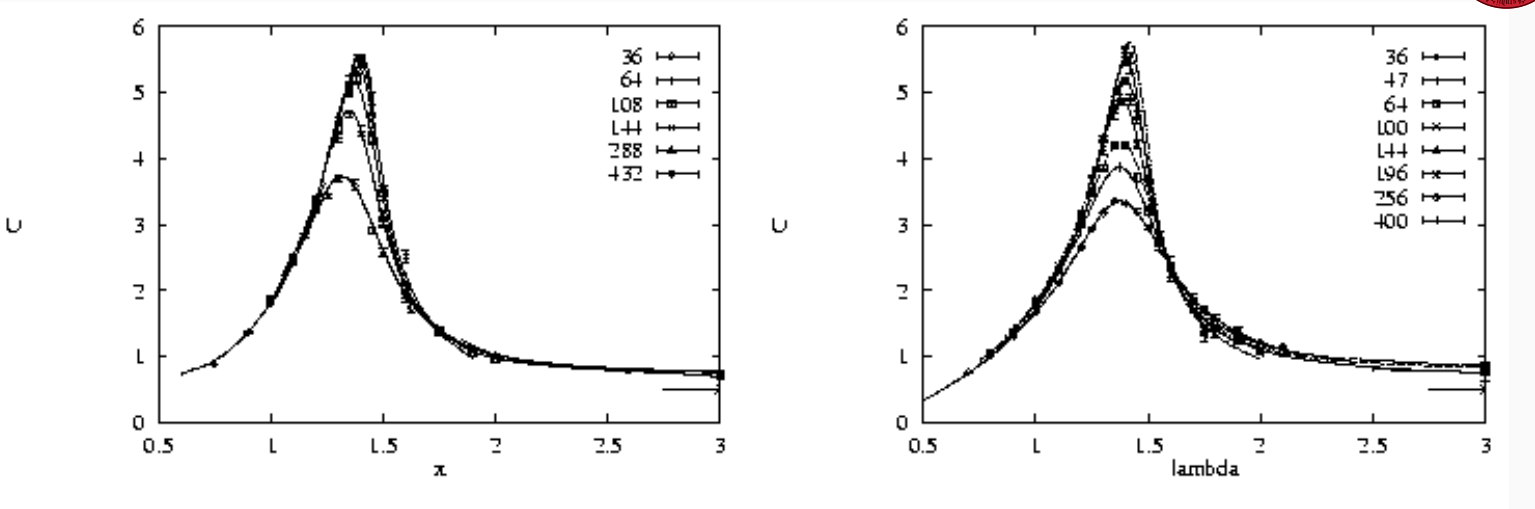

Figure 12: *Specific heat C (edge extrinsic curvature part) of the sphere (left part) and of the torus (right part).*

Membranes and Folding V

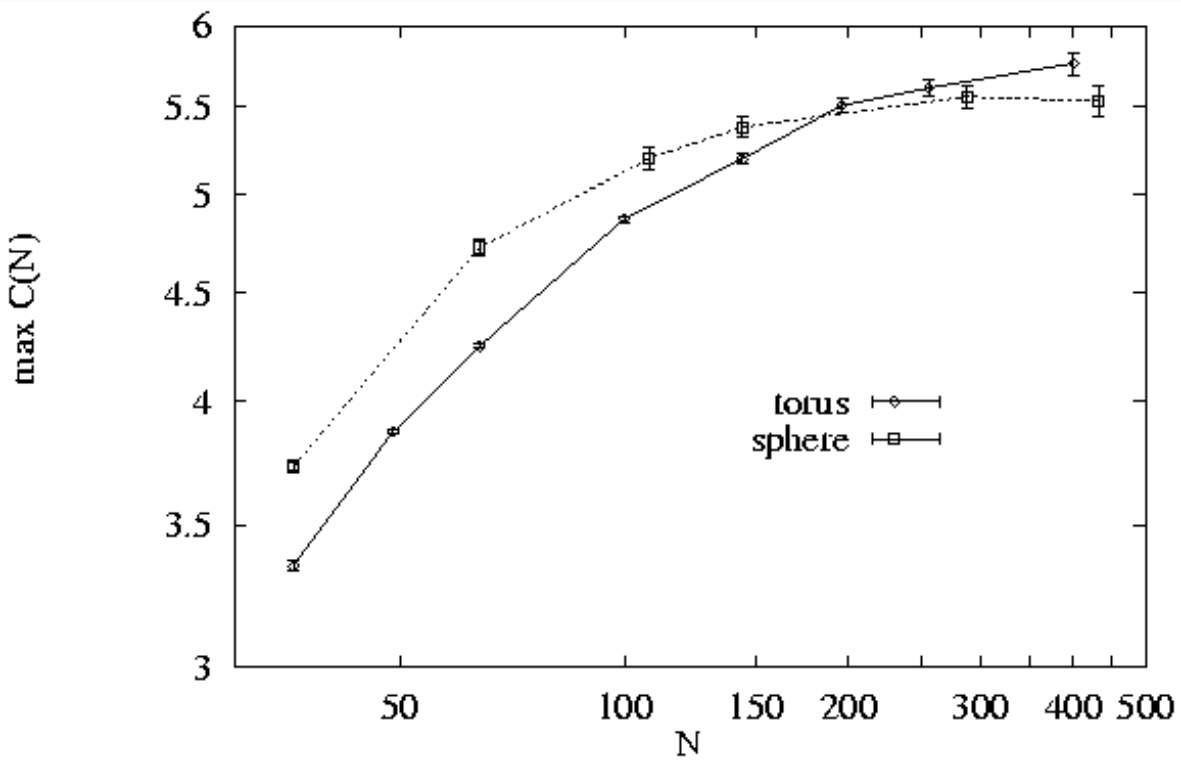

Figure 13: *Maximum of the specific heat* C_N^{max} *of the torus* ($\diamond$) *and the sphere* ($\square$)

- Using the data of the specific heat obtained by applying the extrapolation method, we can get a very accurate estimate of the positions of the maxima and of the heights.

- Figure 13 shows C_N^{max} of the torus and the sphere.
- A change to L^d behaviour is very unlikely and for that reason the data strongly suggest a continuous phase transition in agreement with previous work [14, 20–23, 41, 42].
- From the data shown in Figure 13 we can obtain the following upper boundaries of critical exponents

$$\text{Sphere:} \frac{\alpha}{\nu d} \leq 0.00 \pm 0.04 \qquad \text{Torus:} \frac{\alpha}{\nu d} \leq 0.06 \pm 0.02 \; . \tag{19}$$

- Using this simple method, we cannot distinguish a diverging specific heat with very small but positiv α, a logarithmic divergence $\alpha_s = 0$ and a power law cusp $\alpha_s < 0$, where α_s denotes the exponent of the singular part of the specific heat.
- We will use the abbreviation α instead of α_s.
- Following Fisher [43], these three cases may be distinguished with a fit of the form

$$C(\Delta\lambda) = A \cdot \frac{1}{\alpha}\left(\Delta\lambda^{-\alpha} - 1\right) + B \quad , \quad \Delta\lambda = \left|\lambda_c^N - \lambda\right| \; . \tag{20}$$

- Figure 14 shows such fits for $\alpha = 0.1$ (power law), $\alpha = -0.01$ (near logarithmic) and $\alpha = -1.2, -2.0$ (power law cusp).

- The fits clearly favour a power law cusp of the specific heat with a large negative value of α, although we were not able to estimate the exponent α precisely.

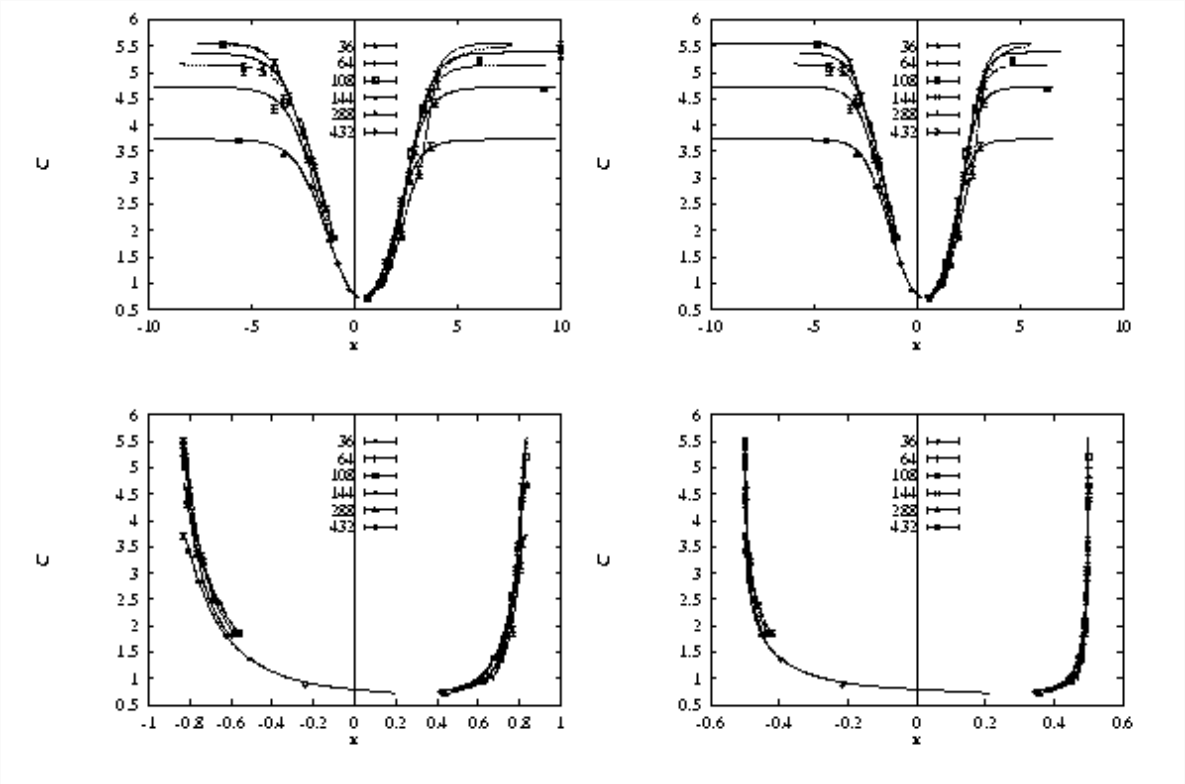

Figure 14: *Plot of the specific heat C against* $x = \frac{1}{\alpha}\left(\Delta\lambda^{-\alpha} - 1\right)$ *with* $\alpha = 0.1$ *(upper left),* -0.01 *(upper right),* -1.2 *(lower left) and* $\alpha = -2.0$ *(lower right).*

- Another possibility to determine the order of the transition is the cumulant $\mathcal{V}_N$ of the edge extrinsic curvature

$$\mathcal{V}_N := 1 - \frac{1}{3}\frac{\langle {\mathcal{H}_e}^4 \rangle_N}{\langle {\mathcal{H}_e}^2 \rangle_N^2} \ , \tag{21}$$

  which behaves quite differently at temperature driven first- and second-order transitions [36, 37] :

$$\text{1. and 2.order:} \quad \mathcal{V}_N|_{min} \overset{N\to\infty}{=} \frac{2}{3} \qquad T \neq T_c \text{fixed} \tag{22}$$

$$\text{2.order:} \quad \mathcal{V}_N|_{min} \overset{N\to\infty}{=} \frac{2}{3} \qquad T = T_c(N) \tag{23}$$

$$\text{1.order:} \quad \mathcal{V}_N|_{min} \overset{N\to\infty}{=} 1 - \frac{2\left(E_+^4 + E_-^4\right)}{3\left(E_+^2 + E_-^2\right)^2} \qquad T = T_c(N) \tag{24}$$

- E_+ and E_- are the energies of the system above and below the transition.
- For a very weak first-order transition ($E_+ \approx E_-$) we also have $\mathcal{V}_N|_{min} \approx 2/3$.
- We computed $\mathcal{V}_N$ defined by equation (21) using again the method of Ferrenberg and Swendsen [39, 40].

- The resulting figures show the predicted single peak minima with wings following equation (22).
- The finite size dependence of the minima of $\mathcal{V}_N|_{min}$ shown in Figure 15 distinctly favours the asymptotic behaviour in equation (23) and therefore a continuous phase transition or a very weak first order transition.

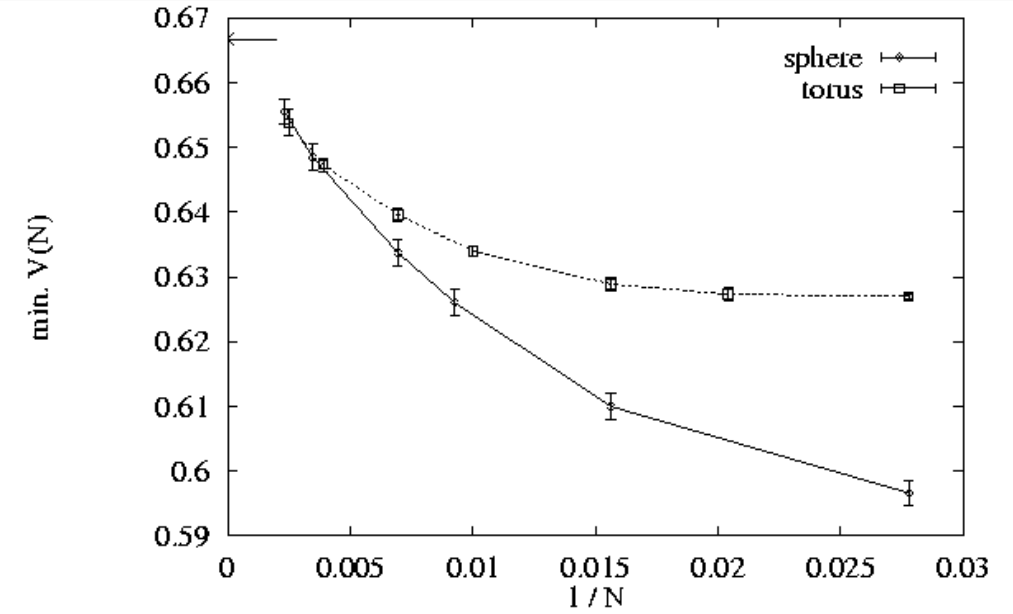

Figure 15: *Finite size dependence of the minimum $\mathcal{V}_N|_{min}$ of the reduced cumulant of the edge extrinsic curvature. ($\diamond$) denotes data of the sphere, ($\square$) those of the torus and the arrow the large N limit 2/3 of a continuous transition.*

- In general, finite size scaling predicts also a shift $\Delta\lambda = \lambda_c^N - \lambda_c^\infty$ of the effective transition 'temperature' λ_c^N proportional to $N^{-1} (= L^{-d})$ for a first- and proportional to $N^{-1/\nu d} (= L^{-1/\nu})$ for a second-order transition.
- Unfortunately λ_c^∞ of dynamically triangulated random surfaces is not known.
- For that reason, we have to use a two-parameter fit with unknowns λ_c^∞ and νd.
- But we can improve the reliability of this fit, because we know more.
- First, the fit has to be a straight line (neglecting corrections to scaling) and we have $\lim_{N\to\infty} \Delta\lambda(N) = 0$.
- Second, the shift $\Delta\lambda(N)$ is different for the specific heat and the cumulant in general.
- Therefore the slope of the fitted lines will be different in general, but we still have $\lim_{N\to\infty} \Delta\lambda(N) = 0$ for both observables.

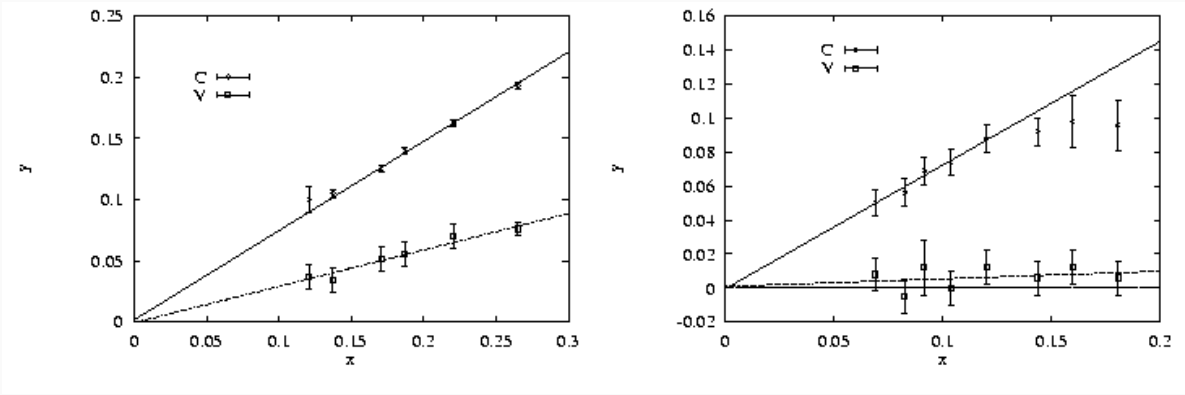

Figure 16: *Best fit of $y = \Delta\lambda$ against $x = N^{-1/\nu d}$ for the sphere (left part) and the torus (right part). ($\diamond$) denotes the specific heat C data, ($\square$) those of the cumulant $\mathcal{V}$.*

- Figure 16 shows the best fits for the sphere and the torus.
- The estimates of the parameters are

$$\lambda_c^{\infty} = 1.51 \pm 0.04 \quad , \quad \nu d = 3.2 \pm 0.5 \tag{25}$$

for the sphere and

$$\lambda_c^{\infty} = 1.47 \pm 0.02 \quad , \quad \nu d = 2.5 \pm 0.5 \tag{26}$$

for the torus.

- We turn now to the order parameter itself. Common practise is to take $\zeta = R/L$ (R is the typical radius, L the linear size of the membrane) to be a suitable order parameter [44, 4, 45–49].
- Initially [49] it was also defined as $R_g(L) = \zeta L$ ($L \to \infty$), with the linear size L of the hexagon and the radius of gyration $R_g^2 \propto \sum_{ij} \left\langle |X_i - X_j|^2 \right\rangle$.
- A suitable choice for the order parameter therefore is

$$\zeta := R^2/N \tag{27}$$

with

$$R^2 = \frac{1}{N(N-1)} \left\langle \sum_{i,j}^{N} \sigma_i \sigma_j (\vec{X}_i - \vec{X}_j)^2 \right\rangle \tag{28}$$

σ_i denotes the number of nearest neighbours, i.e. the number of links connected to a node i.

- The associated susceptibility is

$$\chi_{R^2} := L^d \left(\langle \zeta^2 \rangle - \langle \zeta \rangle^2 \right) = \frac{1}{N} \left(\langle R^4 \rangle - \langle R^2 \rangle^2 \right)$$

- Figure 17 shows the order parameter ζ and Figure 18 the susceptibility of the sphere.
- The results for the torus are similar.

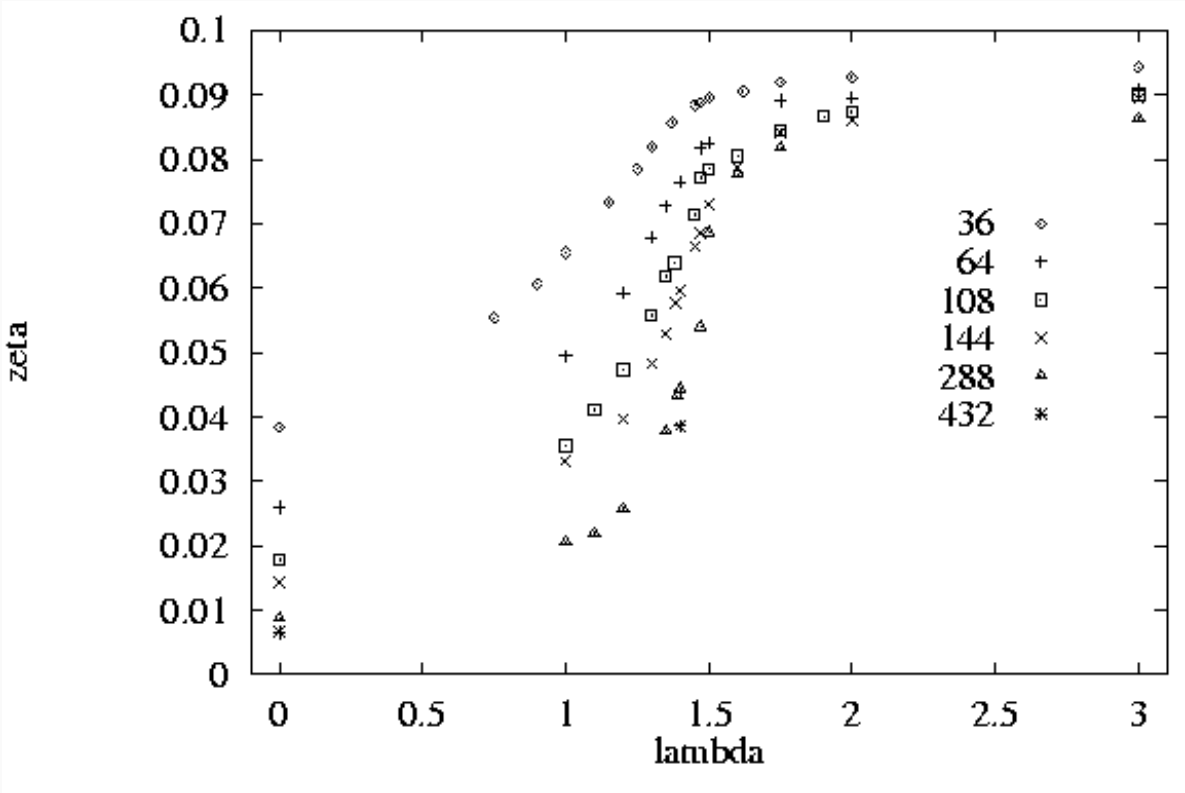

Figure 17: *Order parameter $\zeta = R^2/N$ of the sphere. Errors are smaller than symbol size.*

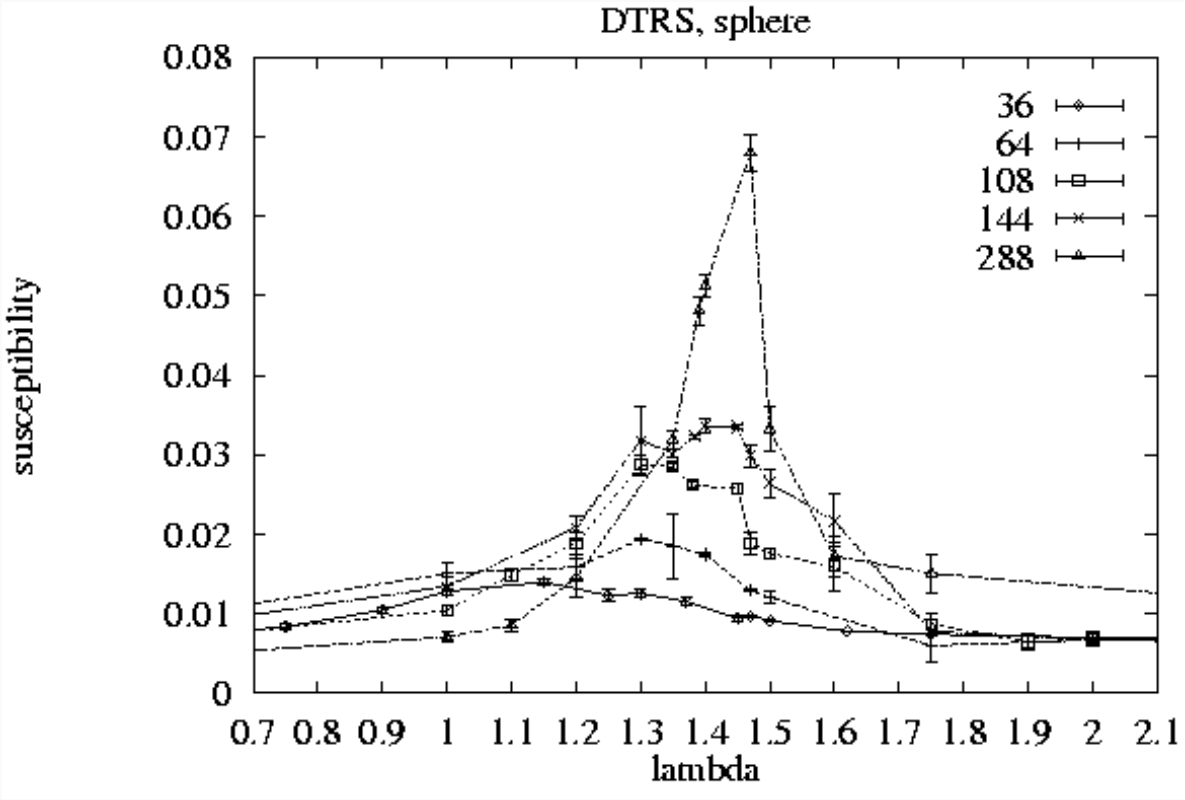

Figure 18: *Susceptibility χ_{R^2} of the sphere (Lines to guide the eye).*

- Another possible order paramter $\zeta' = \langle R'^2 \rangle / N$,

$$\langle R'^2 \rangle = \frac{1}{N} \left\langle \sum_i^N \left(\vec{X}_i - \overline{\vec{X}} \right)^2 \right\rangle$$

  which exhibits a small increase near the phase transition and a slower decay of ζ' for $\lambda \to 0$.
- The difference is caused by a change of the internal geometry near the phase transition [35].
- With the data for the sphere in Figure 17 and the corresponding data of the torus one can estimate the critical exponent $\beta/\nu d$ of the order parameter assuming a second order transition.
- Here we use as the effective critical temperature the position of the peak of the specific heat. C^{max} (c.f. Figure 19).

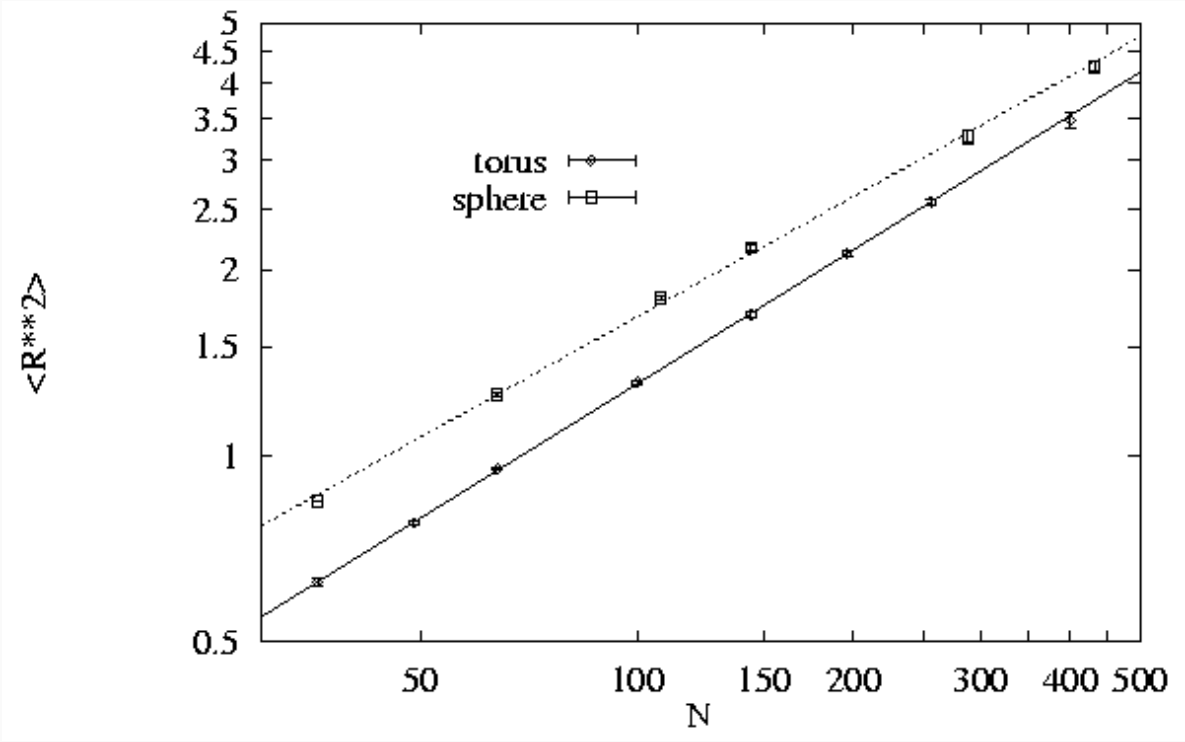

Figure 19: *Scaling of the radius of gyration squared $\langle R^2(N)\rangle$ at the position of the maximum of the specific heat C^{max}. ($\diamond$) denotes the data of the torus, ($\square$) data of the sphere.*

- An estimate of $\beta/\nu d$ using

$$\langle R^2(N, \lambda_c^{eff})\rangle \propto N^{\beta/(\nu d)\,+\,1} \tag{29}$$

results in

$$\text{Torus: } \beta/\nu d = 0.28 \pm 0.02 \quad , \quad \text{Sphere: } \beta/\nu d = 0.35 \pm 0.04 \tag{30}$$

and with the values of νd in equation (25) and (26)

$$\text{Torus: } \beta = 0.7 \pm 0.2 \quad , \quad \text{Sphere: } \beta = 1.1 \pm 0.2 \tag{31}$$

Figure 20 shows the scaling of the maxima of the susceptiblity χ (equation (29), Figure 18).

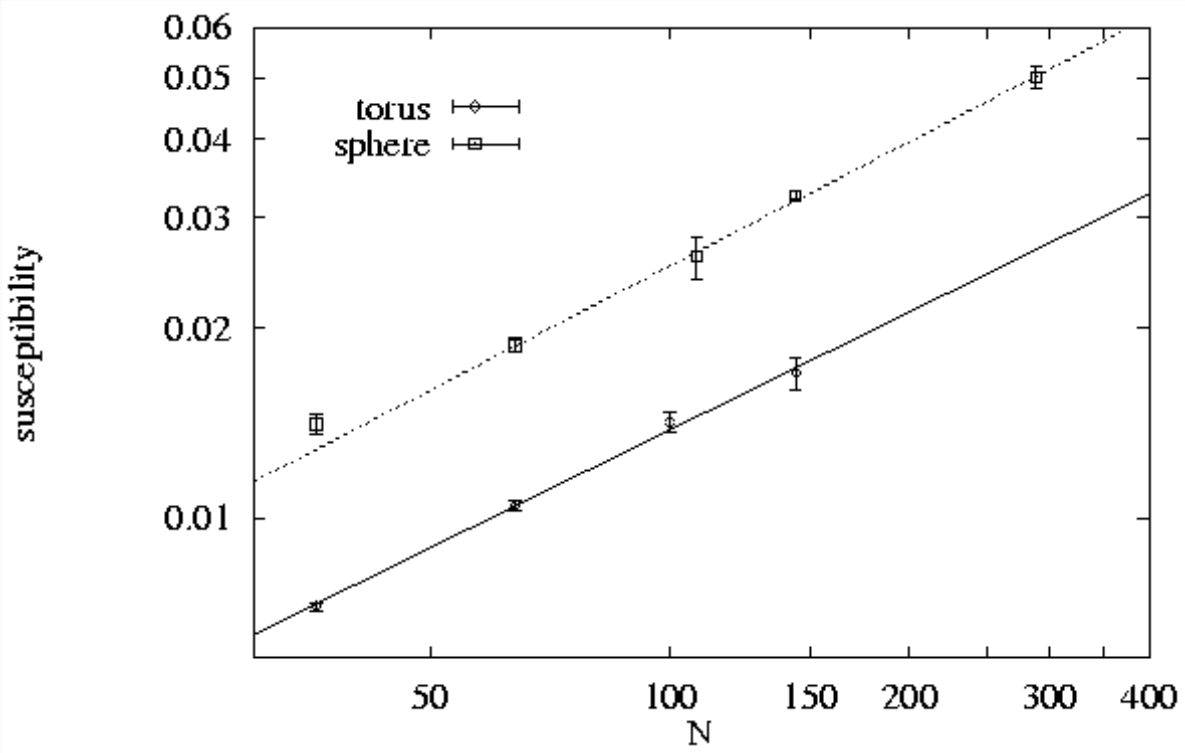

Figure 20: *Scaling of the susceptibility χ (equation (29), Fig. 18) in the case of a torus ($\diamond$) and a sphere ($\square$).*

- The results are

$$\text{Torus: } \gamma/\nu d = 0.62 \pm 0.06 \quad , \quad \text{Sphere: } \gamma/\nu d = 0.66 \pm 0.06 \tag{32}$$

and, using the values of νd in equation (25) and (26),

$$\text{Torus: } \gamma = 1.6 \pm 0.5 \quad , \quad \text{Sphere: } \gamma = 2.1 \pm 0.5 \ . \tag{33}$$

- With these large error bars and estimated values $\alpha \approx -1.5$ the results are almost compatible with the scaling relation

$$\alpha + 2\beta + \gamma = 2 \ . \tag{34}$$

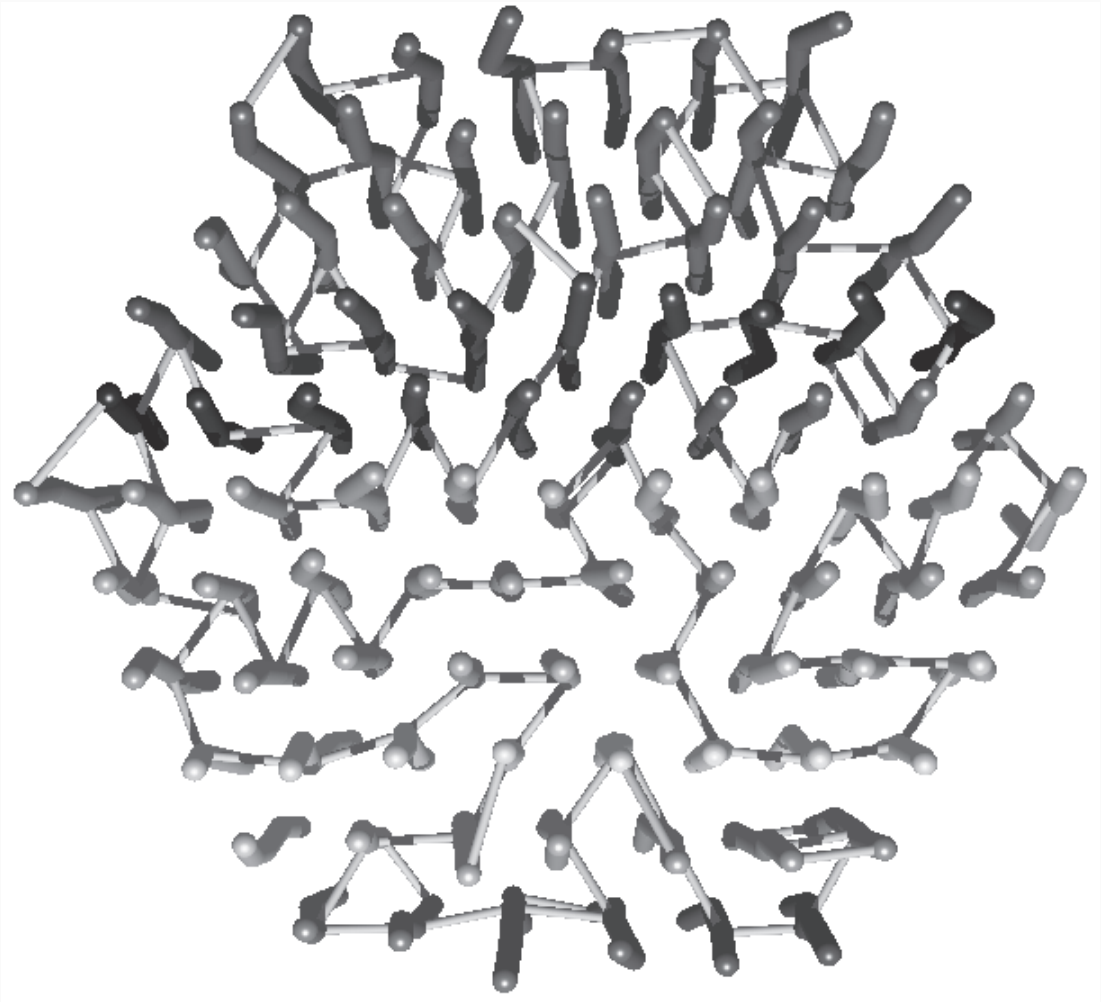

Figure 21: Example of a polymer sheet.

Polymer Sheets II

- Polymers are known to develop various forms, for example linear chains, stars, rings, combs, ladders, three-dimensional networks and branched polymers.
- All these kinds of polymers have linear chains between the branching point.
- The kind of two-dimensional polymers we are studying are compact sheets of monomers, which are linked together periodically with respect to two dimensions.
- Between the branching points there is no chain and the polymers are highly organized sheets.
- The successful "in bulk" synthesis of such two-dimensional polymers was reported recently [50, 51].
- Stupp et al. polymerized self-organized bilayers by two different so-called stitching reactions, which act within three distinct levels of the bilayer. Each oligomer can not have more than two bonds within a layer.
- In addition, not all possible bonds are present, because the stitching reactivity is about 30 to 50% at the upper and lower layer (90% within the middle layer). Is it possible to form a two-dimensional polymer instead of an ensemble of ladder polymers?
- What is the minimal reaction rate, needed for large two-dimensional polymers?
- What kind of structures will be developed at different reaction rates?

- These are questions, which can be answered by percolation theory [52].
- One of the most important results of percolation theory [53, 54] is related to "universality", if the system has short ranged interactions.
- All presently available evidence strongly suggests, that the critical exponents depend on the dimensionality of the lattice only — but not on the lattice structure, boundary conditions and so on.
- The exponents for bond or site percolation, for square, triangular or honeycomb lattices etc. are the same.
- We therefore would expect, that the clusters produced with the above cited stitching reaction also may be described by these exponents.
- Does there exist a large ("infinite") cluster of bonded sites?
- To answer this question, we define the fraction of sites in the largest cluster P_∞ and the probability P_S, that there is a "spanning cluster" of bonds, which connects two opposite boundarys of the underlying lattice.
- Then for an infinite lattice, P_∞ is expected to vanish for $(p - p_c) \to 0_+$ as

$$P_\infty(p) \propto (p - p_c)^\beta \ , \tag{35}$$

where p is the probability, that a bond is present, and p_c is the percolation threshold, above which an infinite cluster exists.

Polymer Sheets IV

- With n_s clusters of size s (number of polymers) the mean size of the finite clusters is related to the percolation susceptibility χ (omnitting the largest ("infinite") cluster)

$$\chi \approx \sum_{s=1}^{\infty}{}' s^2 \, n_s(p) \; , \tag{36}$$

  which diverges at p_c as

$$\chi(p) \propto |p - p_c|^{-\gamma} \; . \tag{37}$$

- Finally, at $p = p_c$ the number n_s of clusters with size s is expected to decay with a power of s:

$$n_s(p_c) \propto s^{-\tau} \; . \tag{38}$$

  Here $\beta, \gamma \text{and} \tau$ are the mentioned exponents.

- Stupp et al. [50] suggest, that they synthesized large two-dimensional polymers.
- Obviously, the effective reaction rate of the stitching reaction has to be larger than the percolation threshold p_c, if one wants to synthesize large sheets instead of ladder polymers.
- Since p_c is not universal, we use a simple but sufficient model of the two-dimensional polymer, to compute p_c. In addition we will measure the exponents.

Polymer Sheets V

- As a model of the two-dimensional polymer we used a stack of three layers, each triangular, hexagonally shaped with free boundaries, as shown in Figure 21.
- At the middle layer, the reaction rate was 100%, i.e. all allowed bonds (two can react) were occupied.
- For that purpose, the bonds of the triangular lattice were choosen successively at random. If the number of bonds of each polymer was less than 2, the randomly choosen bond was occupied.
- Then we stitched the upper and lower layer using the same algorithm, until n_{+1} (n_{-1}) bonds were occupied. n_{+1} (n_{-1}) is the number of occupied bonds of the middle layer n_0 times the stitching probability (reaction rate) p of the upper and lower layer.
- Note, that n_0 is not determined by the linear lattice size L, but may vary slightly for each configuration.
- Because of the restriction, that each polymer may be stitched to at most two neighbours, we do not expect an infinite cluster or percolation at $p = 0$, i.e. without bonds at the upper and lower layer, but an ensemble of linear polymer chains.
- On the contrary, at $p = 1$ all allowed bonds at all three layers are occupied, resulting in an effective coordination number larger than two.

Polymer Sheets VI

- It is worth noting, that even at $p = 1$ the probability, that there is only one cluster containing all polymers, vanishes with increasing system size L.
- Within this model, it is very unlikely to prepare very large perfect two-dimensional polymers.
- If we want to answer the question, if a reaction rate of about 40% is high enough to prepare infinite clusters, we have to determine the percolation threshold.
- As noted, the value of p_c is not universal, but depends strongly on the used lattice and bond restrictions.
- An unbiased way to estimate p_c is to plot the probability P_S of the occurence of a spanning cluster as a function of p for different lattice sizes [**?**].
- The finite size scaling relation for P_S simply reads

$$P_S^{(L)}(p) = \tilde{P_S}\left(\frac{L}{\xi_p}\right) \quad ,$$

  where $\tilde{P_S}$ is the scaling function and ξ_p the correlation length.
- As a consequence, different curves $P_S^{(L)}(p)$ for different choices of L should intersect at $p = p_c$ in a common intersection point $\tilde{P_S}(0)$, apart from corrections to scaling and a bias by the choice of the critical exponents.

- Figure 22 shows this plot for the stitching reaction described above.

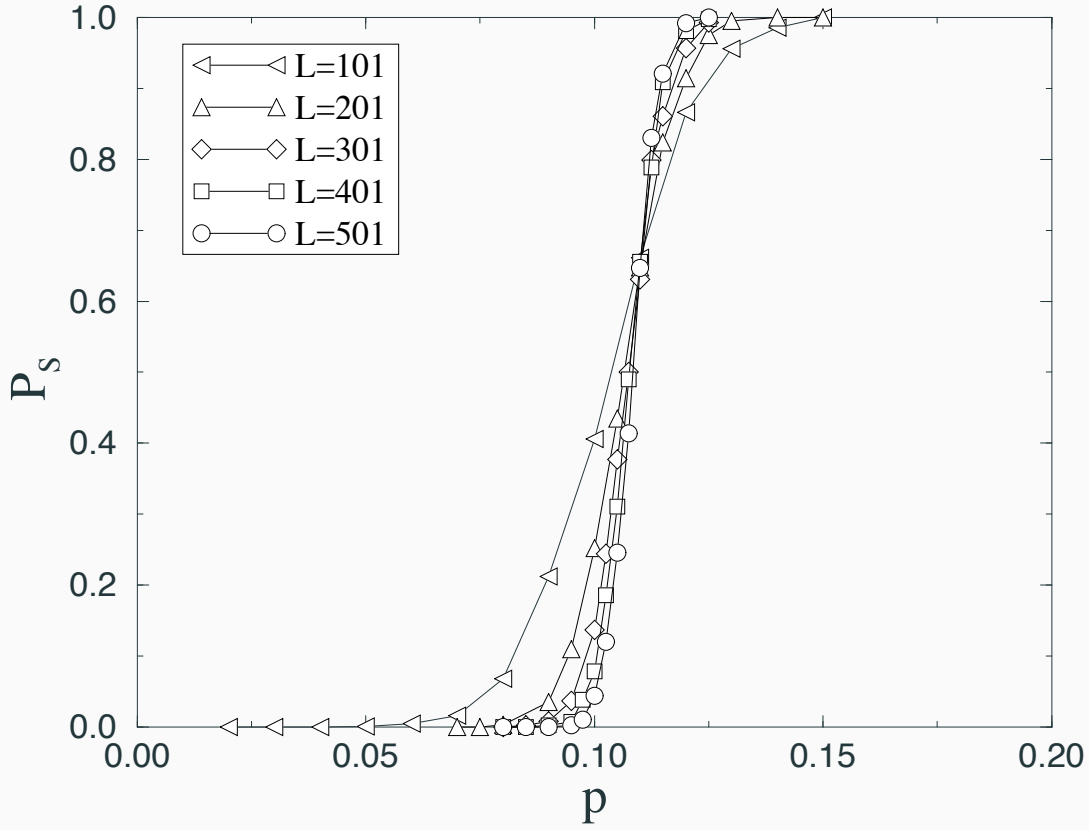

Figure 22: *Unbiased estimate of the percolation threshold* $p_c = 0.110(3)$ *using the spanning probability* P_S.

Polymer Sheets VIII

- From this figure we get one of our main result, the percolation threshold $p_c = 0.110(3)$.
- Hence it follows, that the reaction rate of 30% to 50% reported by Stupp et al. [50] was high enough (within the limits of our percolation model) to prepare an "infinite" two-dimensional polymer.
- Does the percolation of the stitching reaction lie in the same universality class as the standard bond percolation?
- Figure 23 shows a finite size scaling plot of P_∞ using the assumed exact values for $\beta = 5/36$ and $\nu = 4/3$ and p_c obtained from the spanning probability.

Polymer Sheets IX

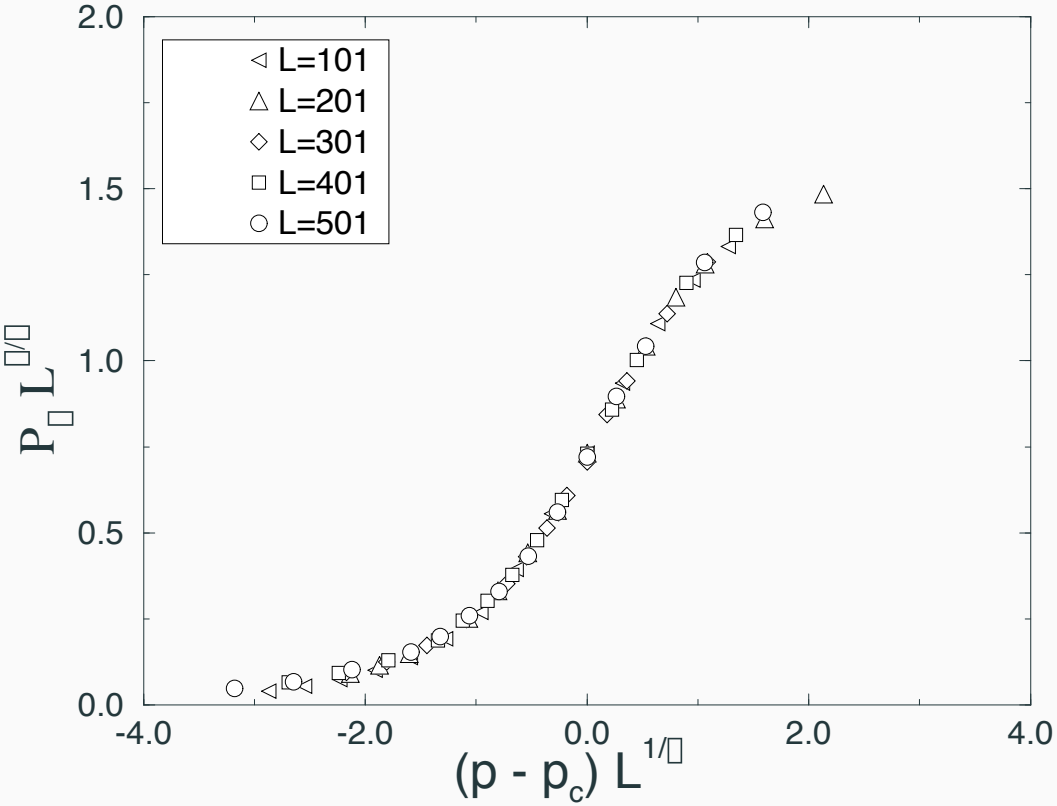

Figure 23: *Finite size scaling of the probability $P_\infty^{(L)}$, which was defined as the fraction of polymers in the largest cluster, with exponents $\nu = 4/3$, $\beta = 5/36$ and $p_c = 0.110(3)$.*

- Within the accuracy of the data, the finite size scaling assumption seems to be fulfilled.

- We may also compare the cluster size distribution to bond percolation.
- Using $\gamma = 43/18$, we plotted the scaling function of the susceptibility χ in figure 24.

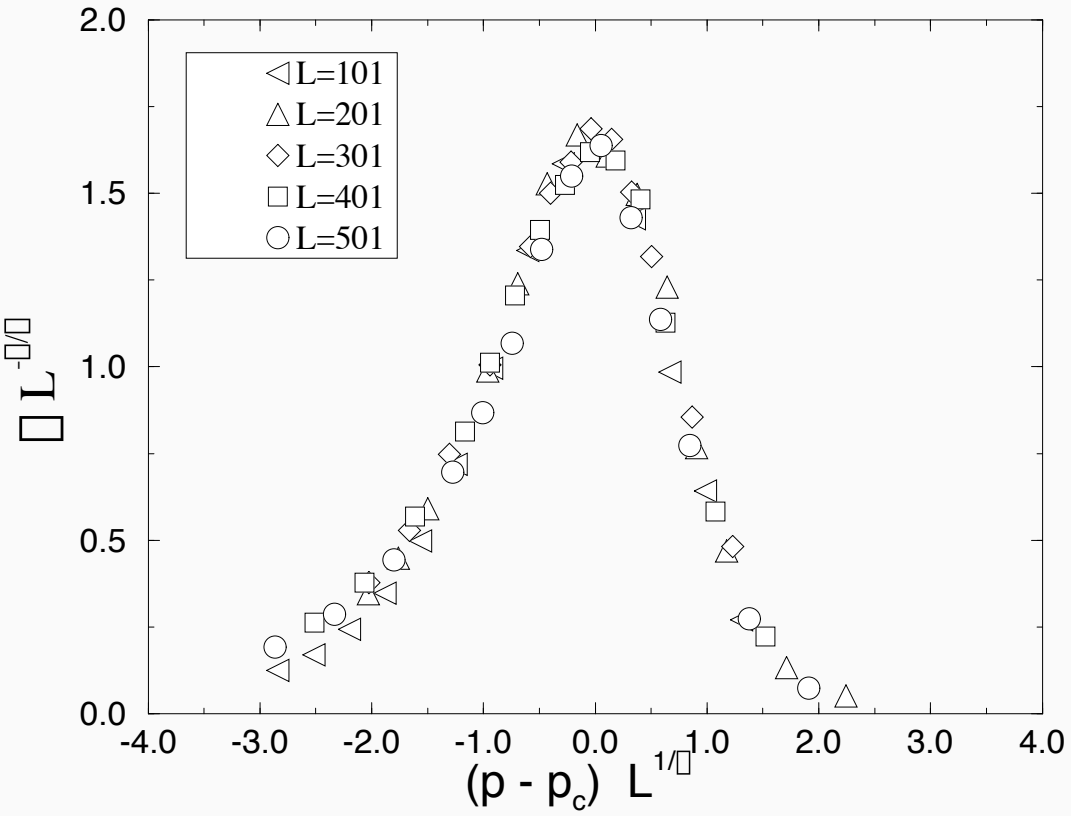

Figure 24: *Finite size scaling of the susceptibility $\chi^{(L)}$ with exponents $\nu = 4/3$, $\gamma = 43/18$ and $p_c = 0.110(3)$.*

- Apart from small deviations of the smallest system far from p_c, the system sizes simulated seem to be in the scaling regime.
- The maximal values of χ vary by orders of magnitude in this range of L!
- Finally, we are interested in the geometric properties of the cluster structure, particularly at the percolation threshold p_c. At p_c the largest (spanning) cluster should form a fractal with Hausdorff dimension d_H.
- This quantity can be defined with the number of polymers N within a sphere of radius R and the relation

$$N = \text{const.} \times R^{d_H} \quad . \tag{39}$$

- Using the data of 1000 configurations of a $L = 1001$ hexagon at p_c, which is shown in figure 25, we measured $d_H(p_c) = 1.91(5)$ in good agreement with the result of percolation theory $91/48 \approx 1.896$.

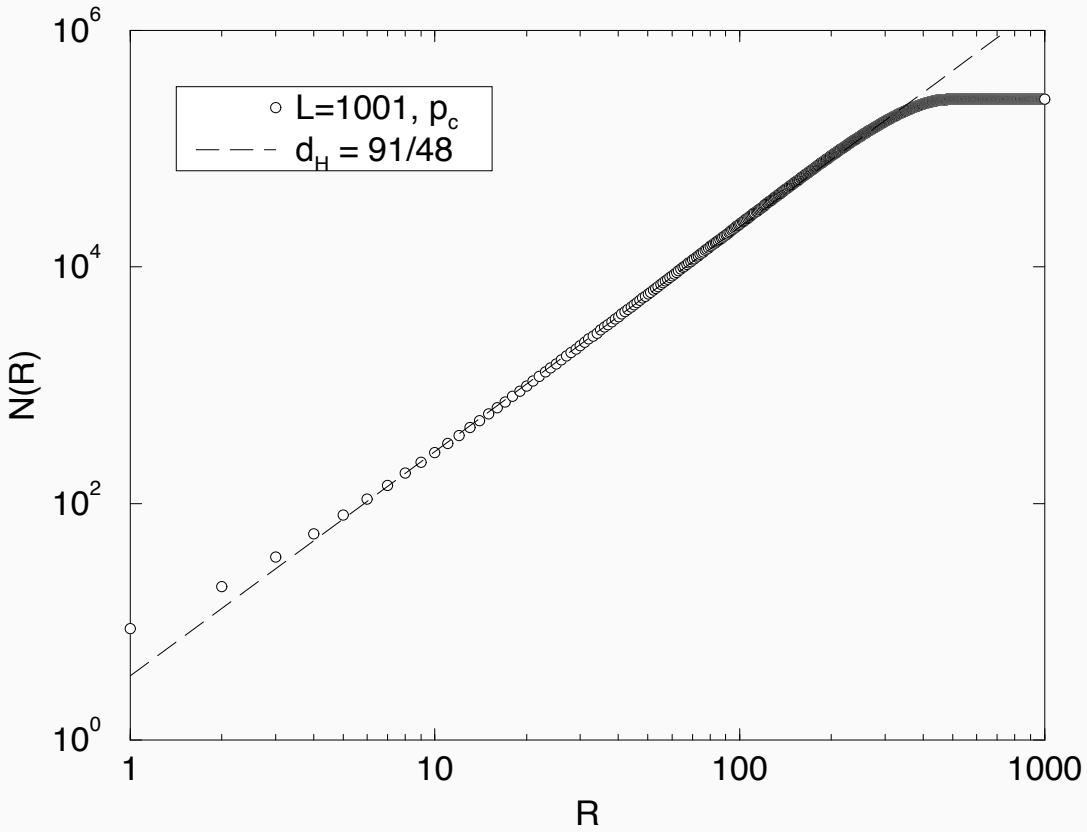

Figure 25: *Number of polymers N within a radius R of the largest cluster. The data of* 1000 *configurations of* $L = 1001$ *hexagons were accumulated. The dashed line has the exact Hausdorff dimension (slope)* $d_H = 91/48$.

Polymer Sheets XIII

- Apart from the largest cluster, there are many smaller ones. Because of the statistical nature of their structure, we restrict ourselves to the number n_s of clusters of size s (which is the number of polymers), which is expected to decrease as a power of s. Within the accuracy of the data, the power law seems to be fulfilled in figure 26.
- Although the Fisher exponent $\tau \approx 1.95(10)$ is somewhat smaller than the expected one 187/91.
- Most probably this is due to the finiteness of the system. High–quality data [**?**] showed, that n_s is less than the expected power law for small s and higher for the largest s.
- Therefore, we underestimated τ systematically.

Polymer Sheets XIV

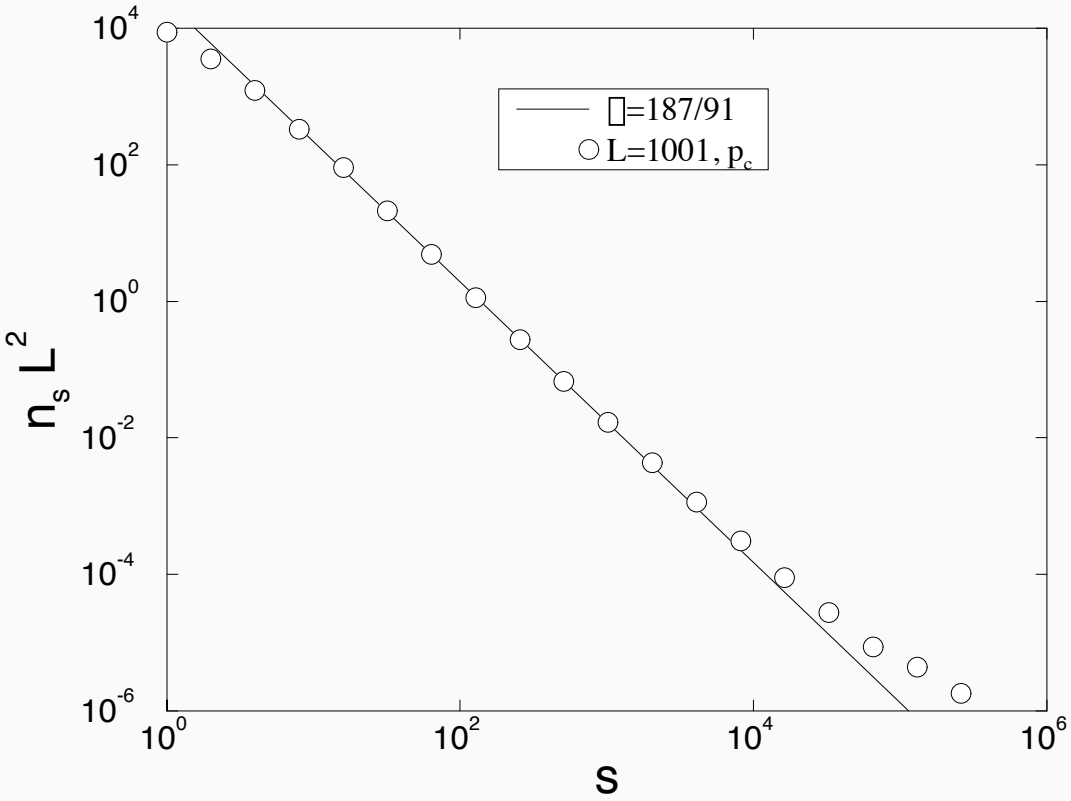

Figure 26: *Cluster distribution of* 1000 *configurations of* $L = 1001$ *hexagon (*751501 *polymers) at the percolation threshold* $p_c \approx 0.110$. *From the slope one computes the Fisher exponents* $\tau \approx 1.95(10)$.

Folding Transition I

- In the absence of self-avoidance, polymerized [55] and fluid [56] membranes adopt a crumpled random structure.
- Theoretical predictions by Flory mean-field approximation and Monte Carlo simulations [55] and renormalization group studies [57] supported the existence of a high temperature crumpled phase for self-avoiding polymerized membranes also, suggesting a possible finite temperature crumpling transition in the presence of an explicit bending rigidity [10].
- However, more extensive computer simulations [4, 58–60] found no crumpling of self-avoiding tethered membranes in a good solvent.
- This prediction was confirmed by experimental studies of graphitic oxide [5].
- On the other hand, polymerized vesicles undergo a wrinkling transition [6], and upon addition of 10 vol % acetone, Spector and co-workers [5] found small compact objects, which appeared to be folded.
- A poor solvent leads to (short-ranged) attractive interactions, and a single membrane was found to be flat for high temperatures [58], but in a collapsed state for sufficiently low temperatures [4].

Folding Transition II

- The transition between the flat and the collapsed states of the membrane proceeds through a sequence of **folding transitions**, which were first found by cooling of a single membrane from the flat phase [44].
- Because no hysteresis was found, it was ruled out that the folded configurations are metastable states.
- However, this method does *not* give sufficient evidence of the order or even the existence of a transition. For instance, hysteresis can also be found at *second order* phase transitions of finite systems and the results for one system size may be misleading. In addition, the experimentally observed wrinkling transition is first order [6].
- Besides the nearest neighbour interactions, the membranes can be modeled similar to those of Abraham and Kardar [44].

Folding Transition III

- The N particles of the polymerized membrane form the sites of a hexagonal shaped triangular lattice.
- The bond potential between nearest neighbour particles is

$$V^{\mathbf{B}} = \sum_{j(i)} \left(b_0 - r_{ij}\right)^2 , \tag{40}$$

with an equilibrium length b_0 and distances r_{ij} between particle i and its nearest neighbors $j(i)$. In place of this harmonic potential, tethers were used by Abraham and Kardar [44].

- All particles interact through a shifted Lennard-Jones potential

$$V_{ij}^{\mathbf{LJ}} = \begin{cases} \left(\frac{1}{r_{ij}^{\mathbf{12}}} - 2\frac{1}{r_{ij}^{\mathbf{6}}}\right) + \left(\frac{1}{r_c^{\mathbf{12}}} - 2\frac{1}{r_c^{\mathbf{6}}}\right) & , \quad r_{ij} <= r_c \\ 0 & , \quad r_c < r_{ij} \end{cases} \tag{41}$$

with a cut-off at $r_c = 2.5$. The repulsive part of this interaction guarantees self-avoidance of the membrane.

Folding Transition IV

- The folding of the membrane can be described by the eigenvalues ${\lambda_1}^2 >= {\lambda_2}^2 >= {\lambda_3}^2$ of the inertia tensor

$$\mathcal{T}_{\alpha,\beta} = \frac{1}{N}\sum_{i=1}^{N}\left(r_{i\alpha}r_{i\beta} - \overline{r}_\alpha \overline{r}_\beta\right) \ , \tag{42}$$

  where $\alpha, \beta \in \{x, y, z\}$, and the sum runs over all particles of a given configuration; $\overline{r}_\alpha$ is the α component of the center of mass for a configuration.

- We can estimate the expected change of the membrane eigenvalues by those of an unfolded or folded disc with radius 1 and width $d = 0.1$ as shown in Table 1.
- Taking into account all three eigenvalues, an unfolded, folded or twice folded configuration can be distinguished.
- A collapsed configuration would be indicated by approximately equal eigenvalues.

Folding Transition V

configuration	$\lambda_1{}^2$	$\lambda_2{}^2$	$\lambda_3{}^2$
disc	0.2543	0.2473	0.00084
disc, folded	0.2524	0.0690	0.00332
disc, folded twice	0.0929	0.0487	0.01330
disc	1.0000	1.0000	1.00
disc, folded	0.9925	0.2790	3.95
disc, folded twice	0.3653	0.1969	15.83

Table 1: Eigenvalues of the moment of inertia tensor of a disc with radius 1 and width $d = 0.1$. In the lower part, all numbers are relative to the values of the unfolded disc.

- At the first folding transition, the eigenvalue λ_1^2 stays constant approximately, while the second eigenvalue λ_2^2 decreases by a factor $c \approx 0.2790$. Therefore, we define an *order parameter m* by

$$\langle m(\beta) \rangle = \left\langle \frac{1}{(1-\sqrt{c})} \left[\frac{\lambda_2(\beta)}{\lambda_2(\beta_0)} - \sqrt{c} \right] \right\rangle , \tag{43}$$

where $\lambda_2(\beta_0)$ is a reference value of an unfolded membrane at β_0 far below the inverse critical temperature β_c.

Folding Transition VI

- At a first order transition, the average order-parameter discontinuously jumps at β_c [38, 36, 37].
- Contrary, at a continuous phase transition we expect a power law behavior of the average order parameter $\langle m \rangle(\beta)$ with an exponent β', i.e. $\langle m \rangle \propto (\beta - \beta_c)^{\beta'}, \beta > \beta_c$ [61–64]. Indeed, the average order parameter $\langle m \rangle$ becomes very steep near β_c with increasing number of particles N (data not shown).
- In principle, one can measure the increase of the slope and compare to the predictions of finite size scaling theory.
- Of course, the slope of $\langle m \rangle(\beta)$ is proportional to the *susceptibility* χ, which can be measured by the fluctuations of m also:

$$\chi(\beta) = L^d \beta \left(\langle m^2 \rangle_L - \langle m \rangle_L^2 \right) . \tag{44}$$

- The susceptibility $\chi(\beta)$ is shown in Figure 27 and the scaling of the maximum $\max \chi(\beta)$ in the inset of Figure 27.

Folding Transition VII

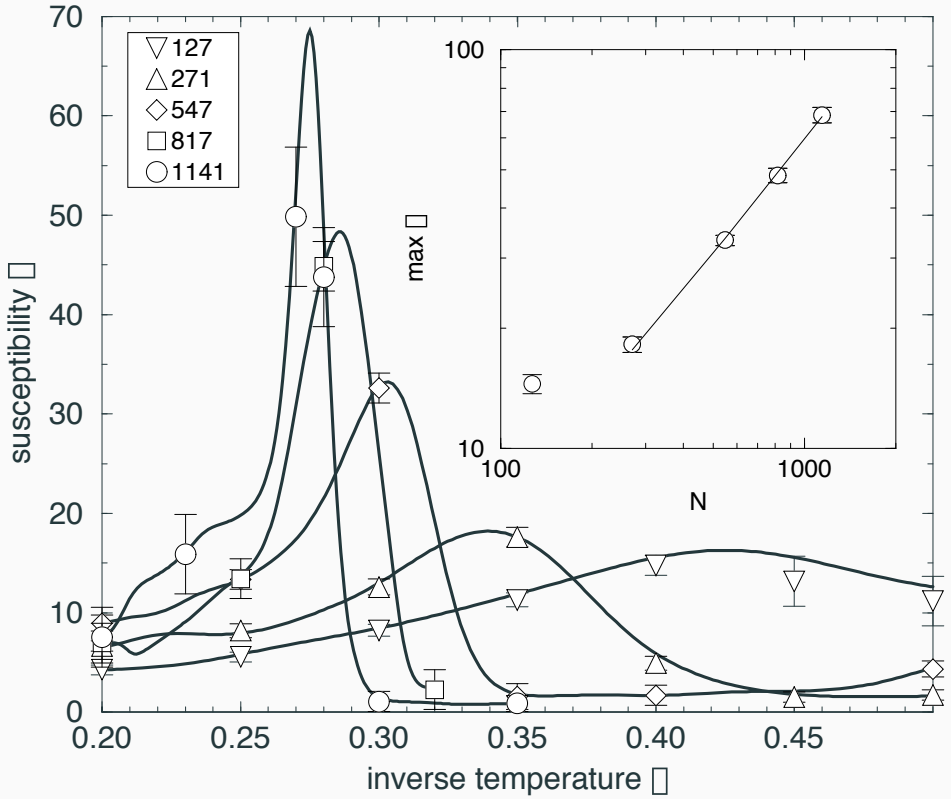

Figure 27: Susceptibility $\chi(\beta)$ for membranes with $N = 127, 271, 547, 817$ and 1141 particles. The solid lines were computed by the multi-histogram method. The scaling of the maximum $\max \chi$ is shown in the inset.

- At a first order transition, $\chi(\beta_c^{\mathbf{eff}})$ is expected to increase proportional to $N = L^d$ [38, 36, 37].

Folding Transition VIII

- At a continuous phase transition, $|\beta - \beta_c|^{-\gamma_\pm}$ is predicted [61–64].
- The L^d increase of $\chi(\beta)$ in Figure 27 gives evidence of the scaling at a *first order* transition.
- In addition, the width of the susceptibility peak should decrease as L^{-d} [38, 36, 37].
- Figure 28 shows a finite size scaling plot of the susceptibility data. Within errors, *first order* scaling behavior can be observed, at least above the inverse transition temperature.

Folding Transition IX

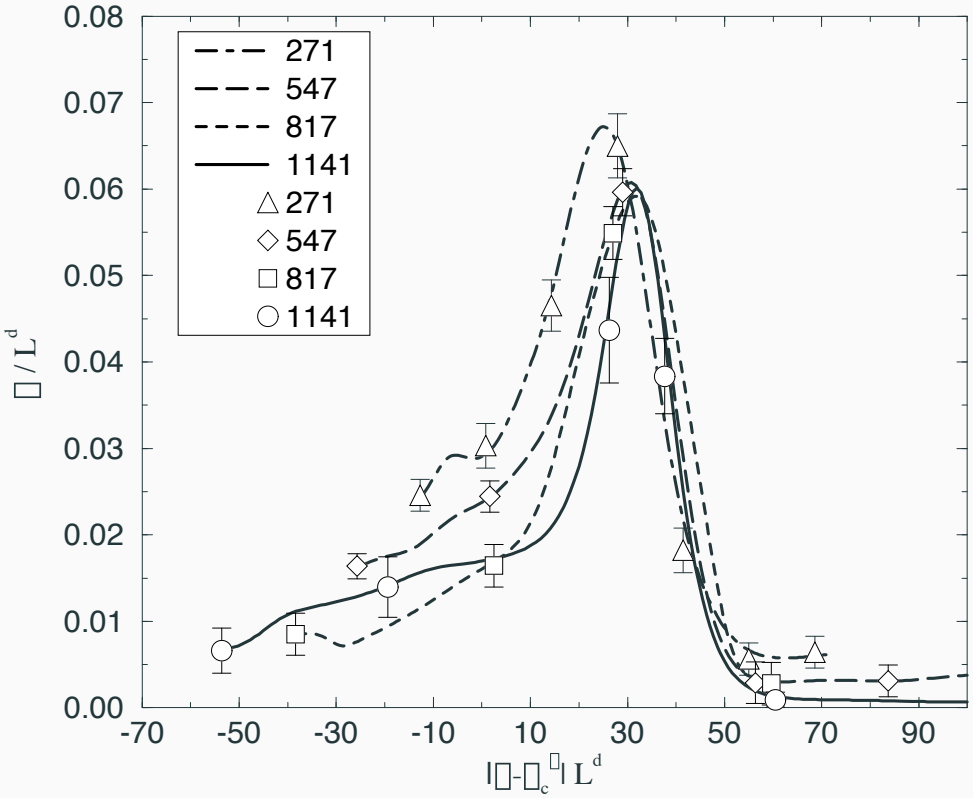

Figure 28: Finite size scaling plot of the susceptibility $\chi(\beta)$ for a first order transition using the value $\beta_c^\infty = 0.247(5)$ from Figure 29.

- The transition temperature β_c^∞ can be extrapolated by the position of the maximum in $\chi(\beta)$ [37], the minimum of the cumulant [37] and the equal weight criterion [65] of the order parameter distribution.

Folding Transition X

- At least for χ, the equal weight criterion predicts a shift of the effective transition temperature proportional to L^{-2d} [66, 65, 67], whereas a shift proportional to $\propto L^{-1/\nu}$ is expected for a continuous phase transition.
- Using quadratic terms in the regression, the extrapolations in Figure 29 of the three observables agree within errors.
- The transition temperature of the first folding transition is found to be $\beta_c^{\infty} = 0.247(5)$.

Folding Transition XI

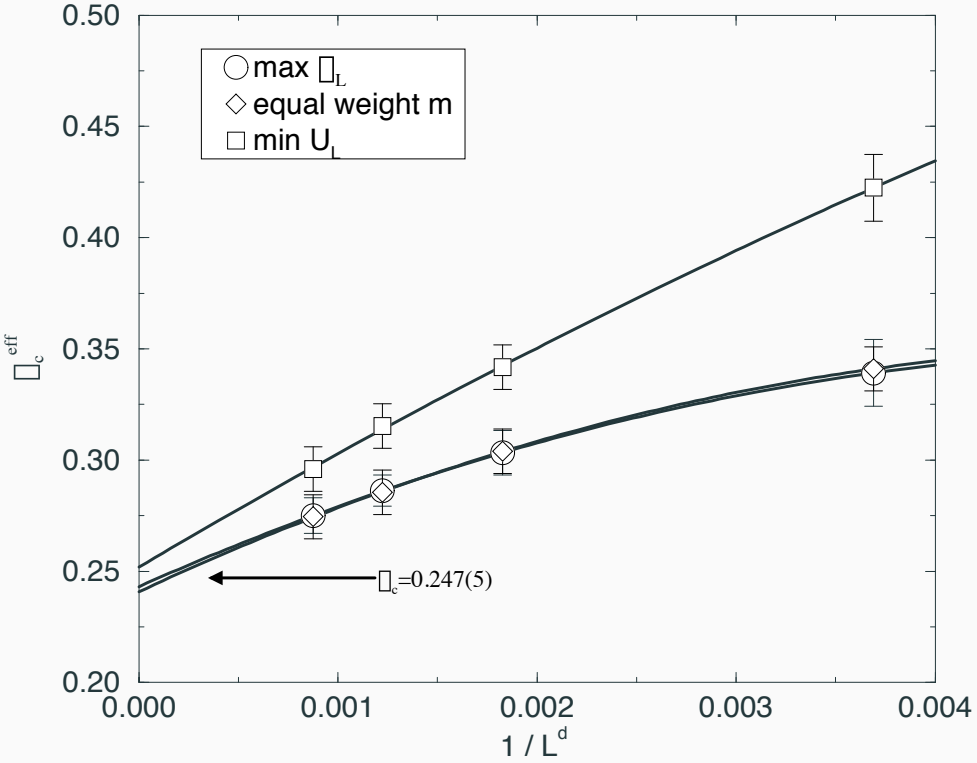

Figure 29: Critical temperature $\beta_c^\infty = 0.247(5)$ determined by the position of the maximal susceptibility χ, the minimum of the cumulant U_L and equal-weight of the order parameter distribution for the four largest system sizes.

- The increase of the susceptibility is caused by the characteristic double-peak structure of the order parameter distribution near β_c, which is typical for a discontinuous phase transition [38, 36, 37, 61, 66, 65, 67, 68].

Folding Transition XII

- Figure 30 shows the expected double-peak distribution $P(m)$ at the equal height transition temperature [65]. The development of a minimum in $P(m)$ is confirmed by the method of Lee and Kosterlitz [68].
- The measured ΔF in the inset of Figure 30 is proportional to the free energy difference at the equal height transition temperature and increases as $(L^d)^x$, $x \approx 1.3$.

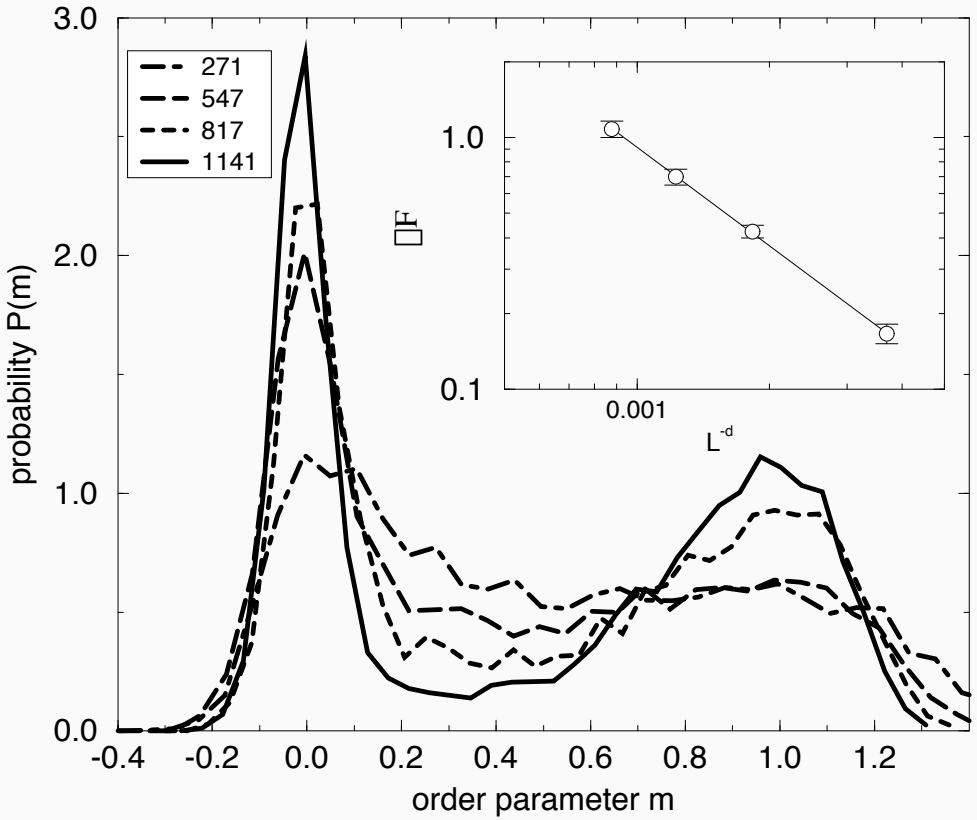

Figure 30: Probability distribution $P(m, \beta_{ew})$ of the order parameter m at the equal-weight transition temperature β_{ew}. The inset shows the free energy difference ΔF at the equal-height transition temperature β_{eh}, which increases $\propto (L^d)^x$, $x \approx 1.3$.

- Further, $P(m)$ can be described by the reduced cumulant U_L

$$U_L(\beta) = 1 - \frac{\langle m^4 \rangle_L}{3\langle m^2 \rangle_L^2} \ . \tag{45}$$

- At a continuous phase transition, $U_L(\beta)$ is expected to approach $2/3$ for all β. The data shows a minimum, which becomes more pronounced for large N, indicating a *first order* phase transition (figure not shown).
- The folding of the membrane must be visible in the attractive part of the potential energy, also. In fact, there is a jump in the potential energy and the related specific heat develops a peak, although very slowly.
- Besides the above defined order parameter, which is based on the geometry of the membrane, we can derive a different order parameter from the attractive part of the Lennard-Jones potential:

$$\tilde{m} = \frac{1}{N} \left\{ \sum_{i<j} \Theta\left(r_c - r_{ij}\right) \left(2\frac{1}{r_{ij}^6} + 2\frac{1}{r_c^6} \right) \right\} \ . \tag{46}$$

Folding Transition XIV

- Compared to m, the order parameter $\tilde{m}$ has the advantage, that it is a local property.
- Figure 31 shows the phase diagram in the (β, h)-plane of a membrane with 271 particles. The first order transition lines were computed by the multi-histogram method [39].
- For the transition from one to two folds, an order parameter similar to m is used, which is based on λ_1 instead of λ_2. $h = 1$ is an upper limit for both transition lines, because of the vanishing attractive interactions at $h = 1$.

Folding Transition XV

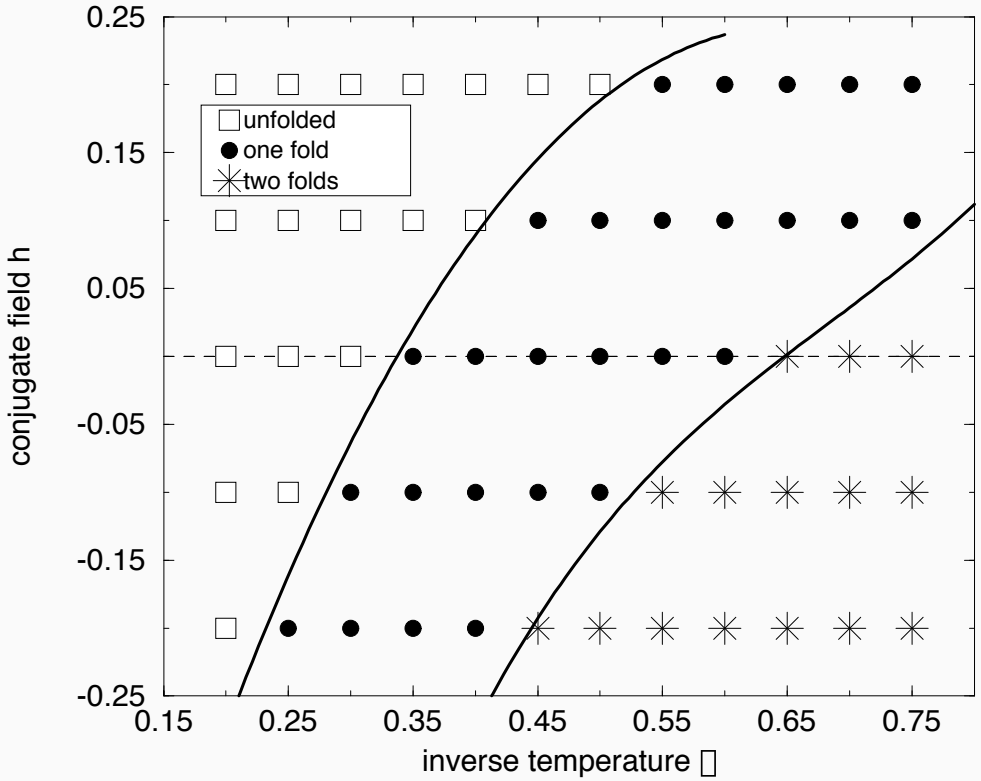

Figure 31: Phase diagram of a membrane with 271 particles in the β, h plane. The symbols denote the result of the simulations, the solid lines are the first order transition lines computed by the multi-histogram method.

- The unfolding of a singly folded membrane bears close resemblance to the unbinding transition of two distinct surfaces.

Folding Transition XVI

- Regarding a folded membrane of N particles, the fraction of particles near the crease decreases with $1/\sqrt{N}$.
- Therefore, the nature of the folding transition is related to the nature of the underlying unbinding transition of two distinct membranes without the crease.
- The shape fluctuations of a single membrane of lateral size $\xi_{\parallel}$ are characterized by the typical fluctuation amplitude $\xi_{\perp} \propto {\xi_{\parallel}}^{\zeta}$.
- Polymerized membranes without lateral tension have a roughness exponent $\zeta \approx 0.6$.
- The steric hindrance of two interacting membranes at separation l leads to an overall loss of entropy, which can be regarded as an effective fluctuation-induced repulsion, $V_{rep} \propto 1/l^{\tau}$ with decay exponent $\tau \approx 3.3$ for polymerized membranes.
- This repulsive interaction causes the unfolding of the membrane even in the presence of attractive van der Waals interactions.
- However, the crease of the folded membrane introduces an additional attractive interaction. This situation is similar to a membrane interaction which exhibits two minima at two different separations.
- Such an interaction implies a *first-order* unbinding transition [69] and may be an explanation of the *first-order* folding transition.

Membrane Proteins

Membrane Proteins: An example I

Rhodopsin as an example:

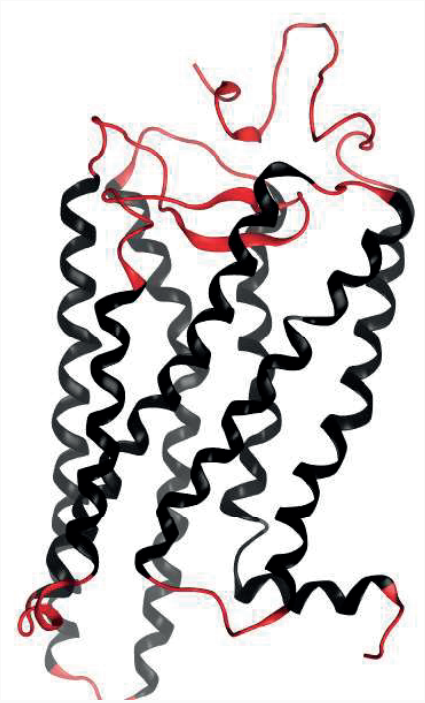

Figure 32: Rhodopsin structure.

- Rhodopsin is a light-sensitive receptor protein.

Membrane Proteins: An example II

- Rhodopsin has seven transmembrane domains.
- Rhodopsin has loops.

- The linker can be mapped onto a coarse grained model.
- This mapping allows extensive studies on the physical properties of the linker.
- There is no bending rigidity so that they appear to be very flexible.
- The loops show generic behaviour.

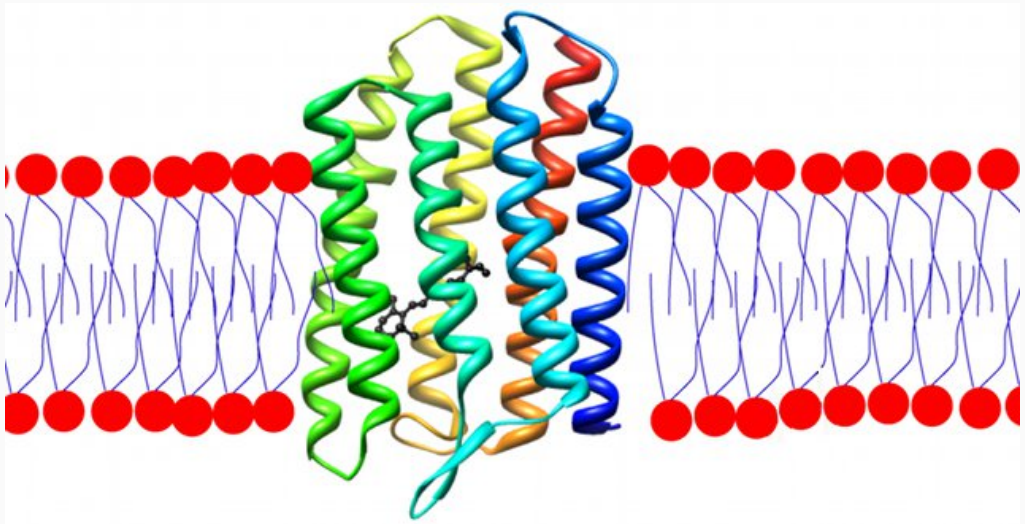

Figure 33: Rhodopsin. Image take from http://wordpress.mrreid.org/2012/01/02/night-vision/.

Membrane Proteins: An example III

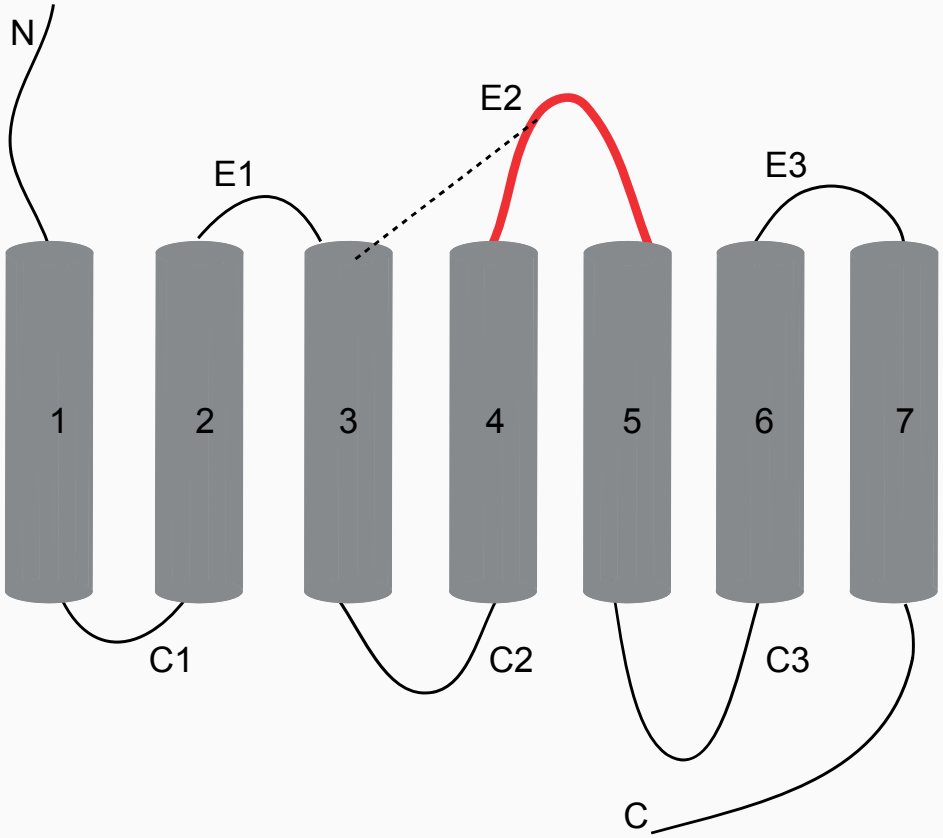

Figure 34: Rhodopsin structure (cnt).

Membrane Proteins: An example IV

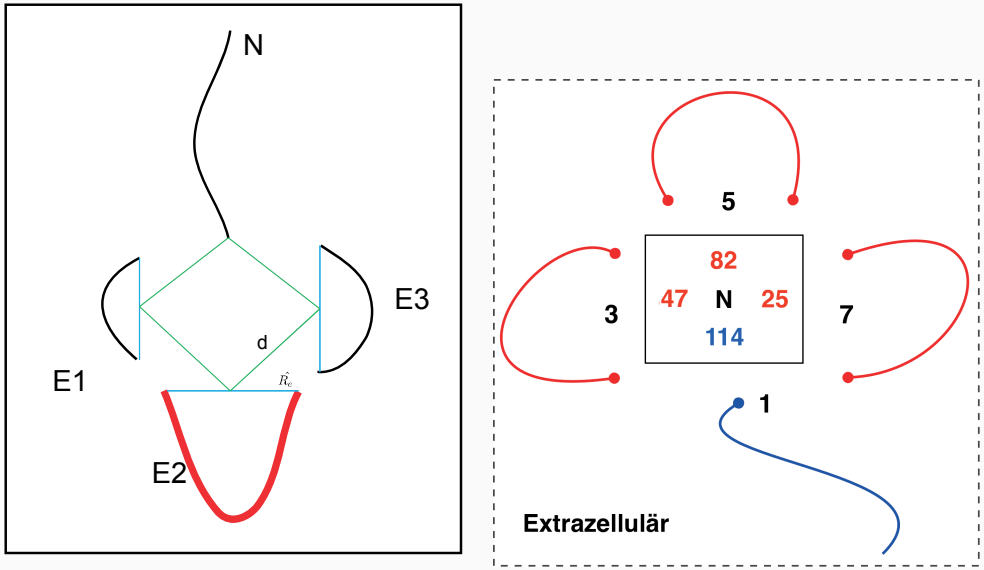

Figure 35: Rhodopsin structure (cnt).

Membrane Proteins: An example V

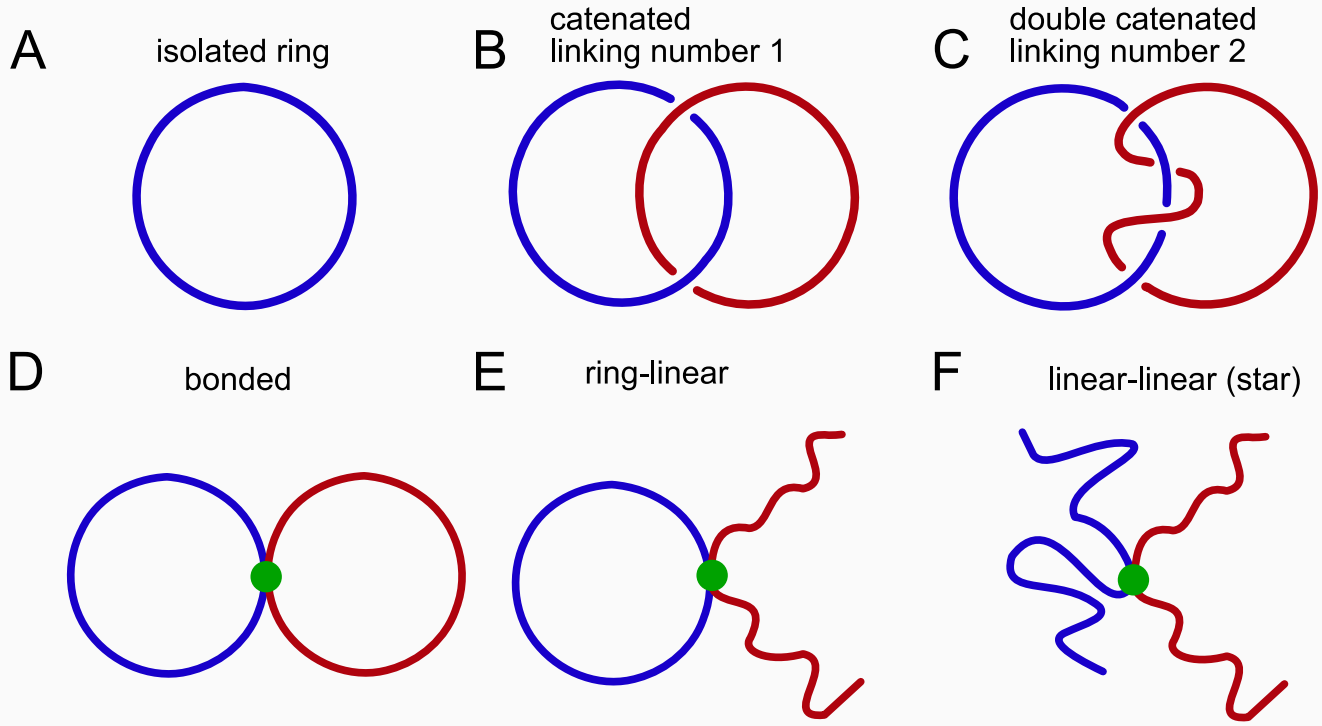

Figure 36: rhodopsin

Membrane Proteins: An example VI

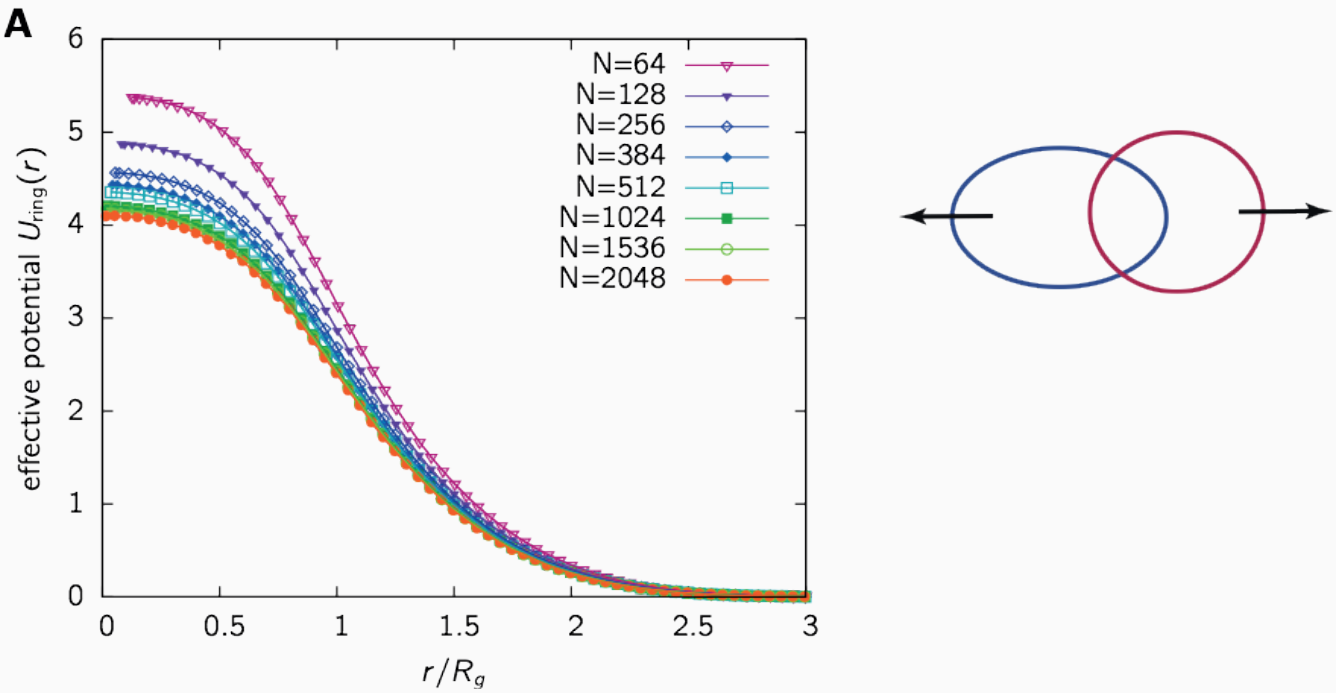

Figure 37: Entropic repulsion of loops.

Membrane Proteins: An example VII

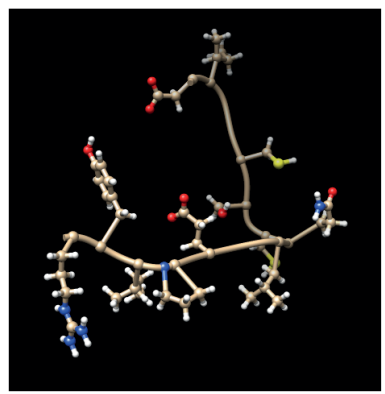

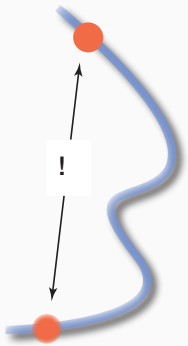

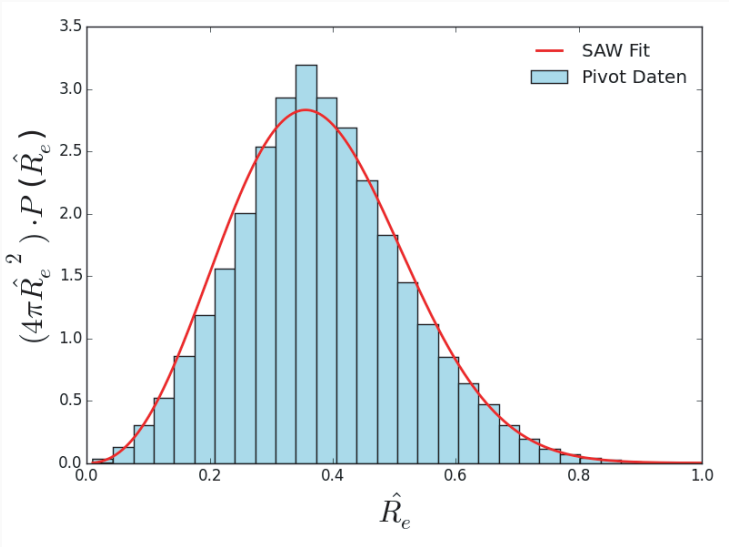

Figure 38: Rhodopsin end-to-end distance.

Membranes and Translocation

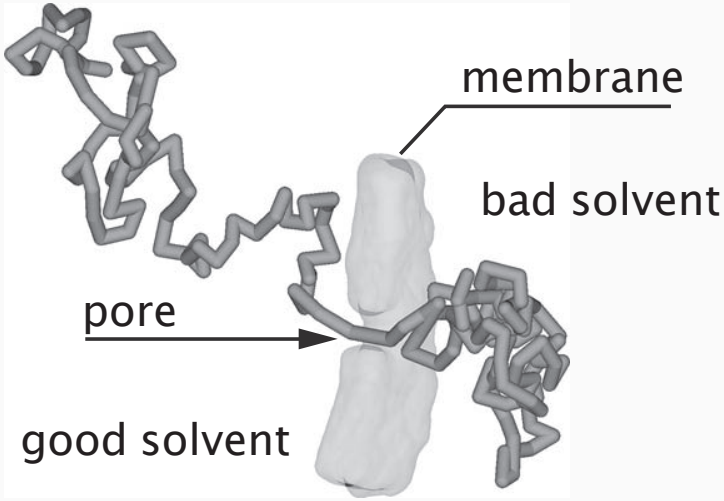

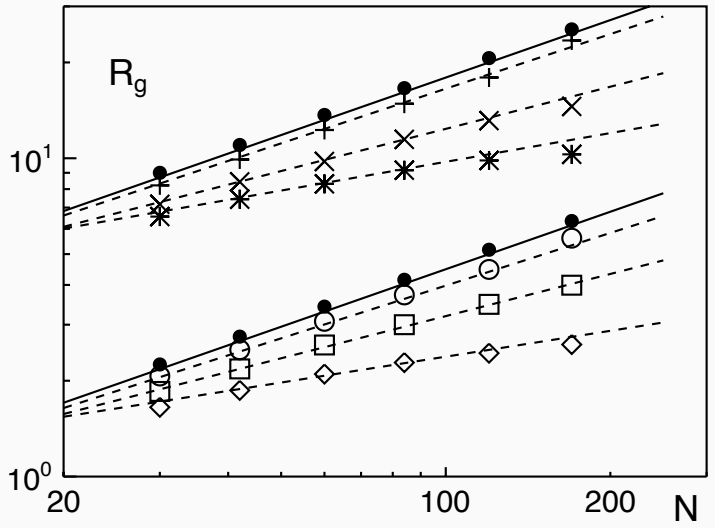

Figure 39: Translocation of a macromolecule through a membrane pore. Image taken from [2]. The radius of gyration of a flexible polymer of length N in good solvent conditions scales as $R_g \sim N^\nu$ with $\nu = 0.61$ (filled circles, full lines). When increasing the solvent-polymer repulsion a_{MS} by Δa (hence decreasing the solvent quality), the scaling of R_g becomes more and more shallow (open symbols). Mimicking bad solvent conditions by reducing the monomer-monomer repulsion a_{MM} by Δa yields similar effects (cross-like symbols). For better visibility the latter data have been shifted by a factor 4.

We shall look at the translocation process including a polymerized membrane with a narrow pore to separate two volumes with potentially different solvent conditions.

For the polymer all beads are subject to a DPD thermostat and a soft-repulsive interaction. For any two beads i and j within an interaction range

$$r_{ij} = |\mathbf{r}_{ij}| = |\mathbf{r}_i - \mathbf{r}_j| \leq r_0 \tag{47}$$

the forces are:

$$\begin{aligned}
\mathbf{F}_{ij}^C &= a_{ij}(1 - r_{ij}/r_0)\,\hat{\mathbf{r}}_{ij} && (48)\\
\mathbf{F}_{ij}^D &= -\gamma_{ij}(1 - r_{ij}/r_0)^2\,(\hat{\mathbf{r}}_{ij} \cdot \mathbf{v}_{ij})\hat{\mathbf{r}}_{ij} && (49)\\
\mathbf{F}_{ij}^R &= \sigma_{ij}(1 - r_{ij}/r_0)\zeta_{ij}\hat{\mathbf{r}}_{ij}\ . && (50)
\end{aligned}$$

Here, ζ_{ij} is an uncorrelated random variable with zero mean and unit variance, $\mathbf{v}_{ij} = \mathbf{v}_i - \mathbf{v}_j|$, and $\hat{\mathbf{r}}_{ij} = \mathbf{r}_{ij}/r_{ij}$.

The unit of length of the simulations is given by the thermostat's interaction range, r_0. The noise strength σ_{ij} is related to the dissipation strength γ_{ij} via the fluctuation-dissipation theorem

$$\sigma_{ij}^2 = 2\,\gamma_{ij}\,k_B\,T\ . \tag{51}$$

To obtain a polymer, beads are connected by FENE bonds, i.e. we imposed a potential

$$U_F(r_{i,i+1}) = -\frac{k(2\,r_0-\ell)^2}{2}\ln\left\{1-\left(\frac{r_{i,i+1}-\ell}{2\,r_0-\ell}\right)^2\right\} \tag{52}$$

with $k_F = 40\,k_B\,T$ and $\ell = 0.7\,r_0$.

The separating membrane is implemented as a double layer of DPD beads connected via simple Hookean springs

$$U_2(r_{i,i+1}) = k_0(|\mathbf{r}_{i,i+1}| - l_0)^2/2 \tag{53}$$

($k_0 = 100\,k_B\,T$, $l_0 = 0.45\,r_0$), and an additional bending stiffness was imposed via a potential of the form $U_3(\mathbf{r}_{i-1},\mathbf{r}_i,\mathbf{r}_{i+1}) = \kappa[1-\cos(\phi)]$, with $\kappa = 10 k_B\,T$ and $\cos\phi = \hat{\mathbf{r}}_{i-1,i}\cdot\hat{\mathbf{r}}_{i,i+1}$.

Membranes and Translocation IV

To model the nanopore, a square of 2×2 'ghost beads' in each membrane layer is given a vanishing interaction with all other beads except the neighboring membrane beads. These ghost beads are hence only involved in calculating the structural forces that established the separating membrane. The nanopore had thus a diameter of roughly r_0.

Membranes and Translocation V

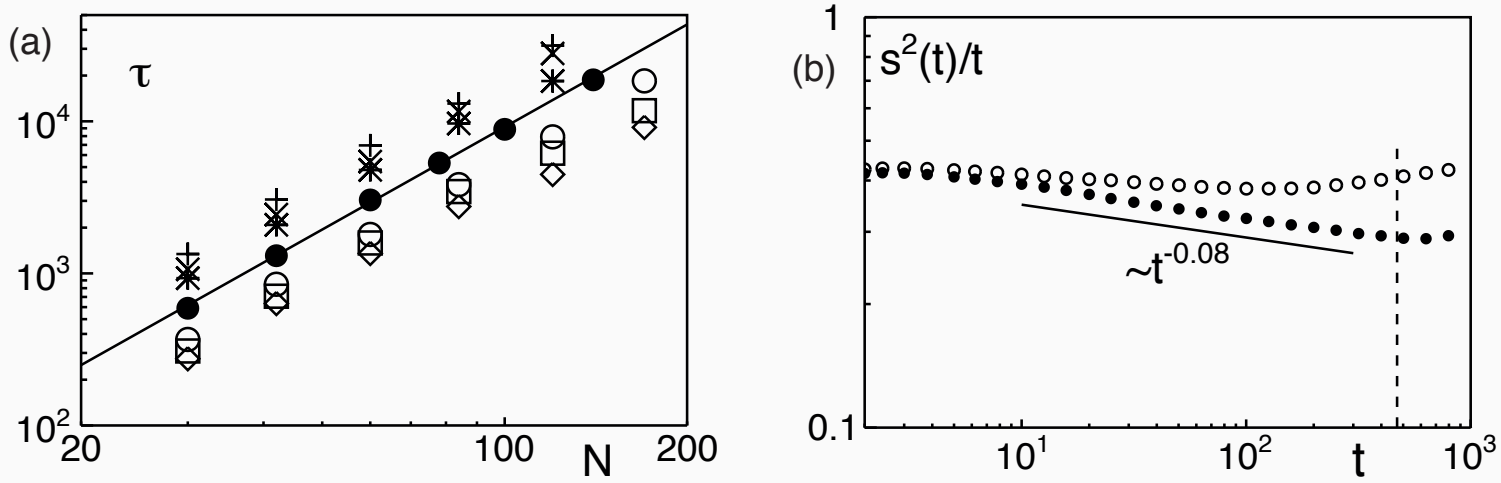

Figure 40: (a) The unbiased translocation time τ for good solvent conditions (filled circles, full line; data shifted by factor 1.5 for better visibility) scales as $\tau \sim N^{\beta}$ with $\beta = 2.33$. This scaling is also observed when decreasing the solvent quality by increasing a_{MS} (open symbols) or decreasing a_{MM} (cross-like symbols; shifted by factor 4). (b) The exponent ν decreases with decreasing solvent quality. Increasing a_{MS} (open circles) and decreasing a_{MM} by Δa from $a_0 = a_{SS} = 25 k_B T$ have similar effects. In contrast to ν the exponent $\beta \approx 2.33$ (dashed line) hardly varies with solvent conditions.

Membranes DNA Interaction

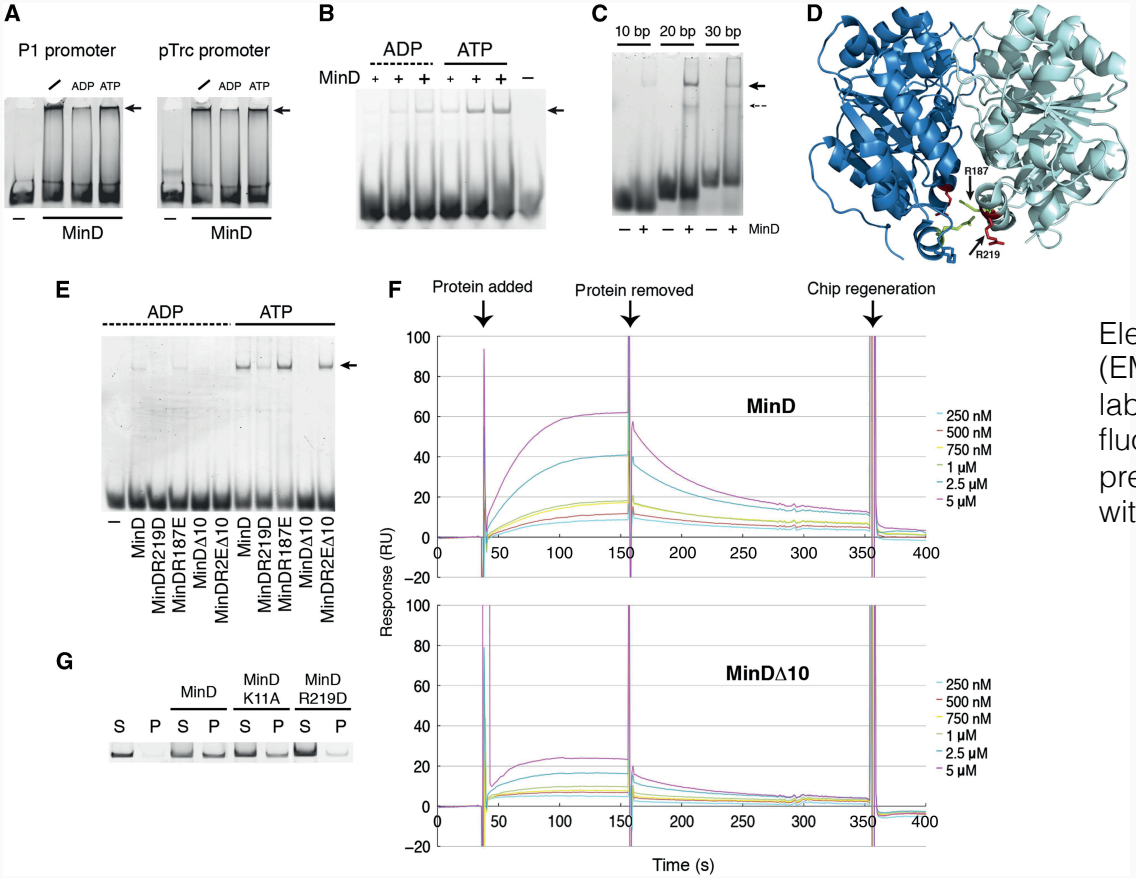

MinD Protein

PBD accession number 3Q9L

Electrophoretic mobility shift assays (EMSAs) of dsDNA fragments (200 fmol) labeled by 50 -hexachloro-6- carboxy-fluoresceine (HEX) incubated in the presence of 1 mM ATP or ADP with or without (minus) MinD.

Figure 41: MinD Protein.

Membranes DNA Interaction II

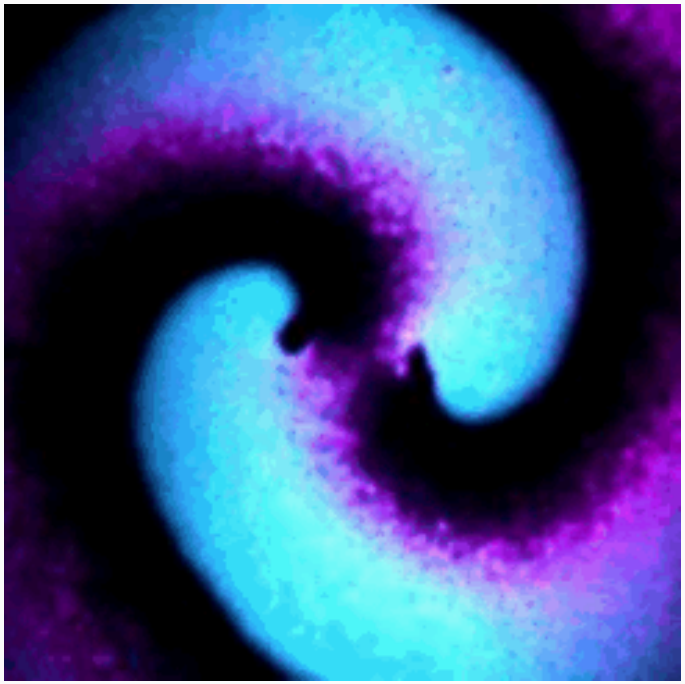

Figure 42: MinD (cyan) chased by MinE (magenta) to form spiraling waves on an artificial membrane. Taken from (https://en.wikipedia.org/wiki/Min_System).

- The model includes two E. coli sister chromosomes described as two self-avoiding ring polymers.

Membranes DNA Interaction III

- Approximating biological "storage" such as the bacterial nucleoid an elongated rectangular cuboid of aspect ratio 1 : 8 comparable to the aspect ratio of the nucleoid [71] confines both ring polymers (representing the replicated sister chromosomes).
- Studying two polymer rings of lengths $N = 80$, the linear dimensions of the confining geometry are set up such that the radius of gyration R_{gyr} of the unconfined chain is larger than the linear square box sizes.
- The choice of parameters (aspect ratio of the cell of 1 : 8 and volume fraction with a single chain only of 10%) reflects the situation for E. coli and its chromosome at the onset of segregation [71].
- An overlapping configuration of two chains is created to initiate the segregation process as is illustrated in Fig. S1. Independent Monte Carlo trajectories (driven by different random number sequences) representing the dynamics of the segregation process are then sampled.
- In order to study the impact of nonspecific DNA tethering to the membrane and to mimic the oscillatory behaviour of the MinD protein MC simulations representing the following biological situations.
  (i) mutant case without possibility of tethering,
  (ii) homogeneous tethering,
  (iii) fixed gradient of tethering probability,

(iv) oscillating tethering probability (representing the MinD oscillations) and
(v) smooth gradient of tethering probability.

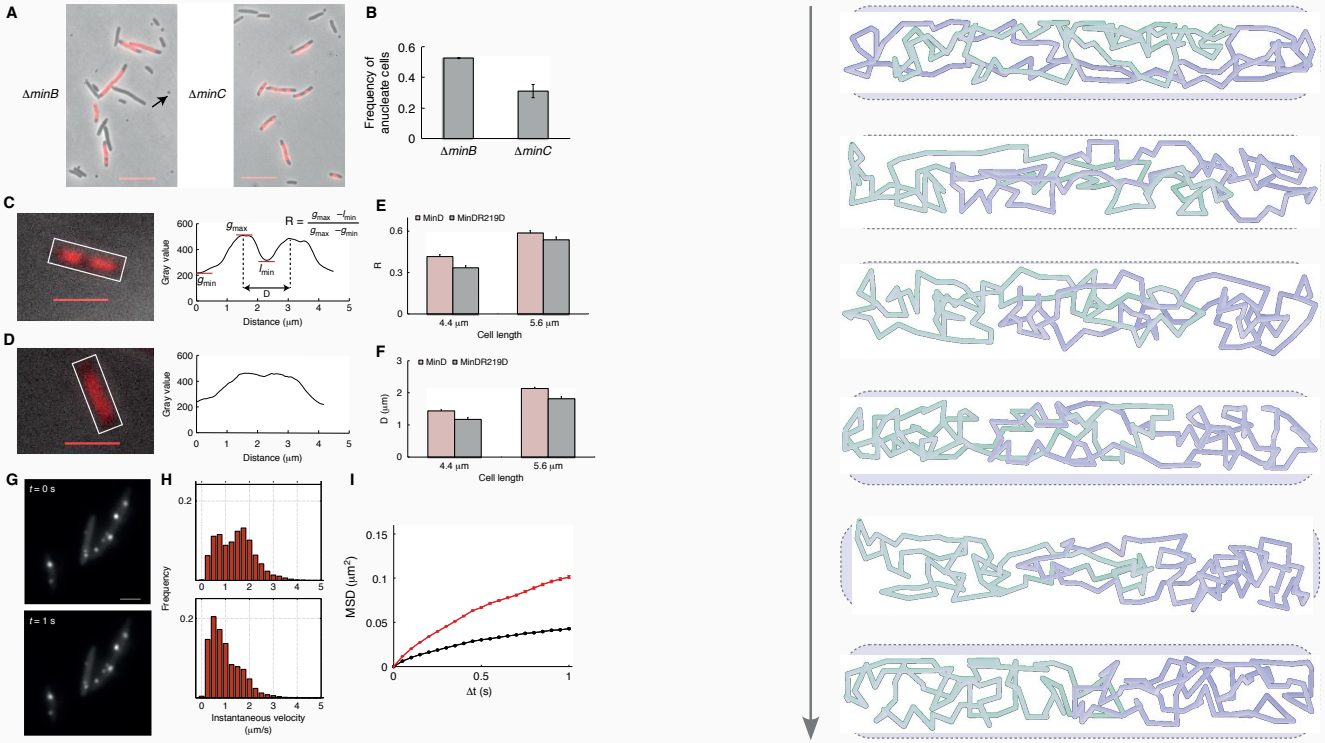

Figure 43: Disentangling of two circular chromosomes.

Membranes DNA Interaction V

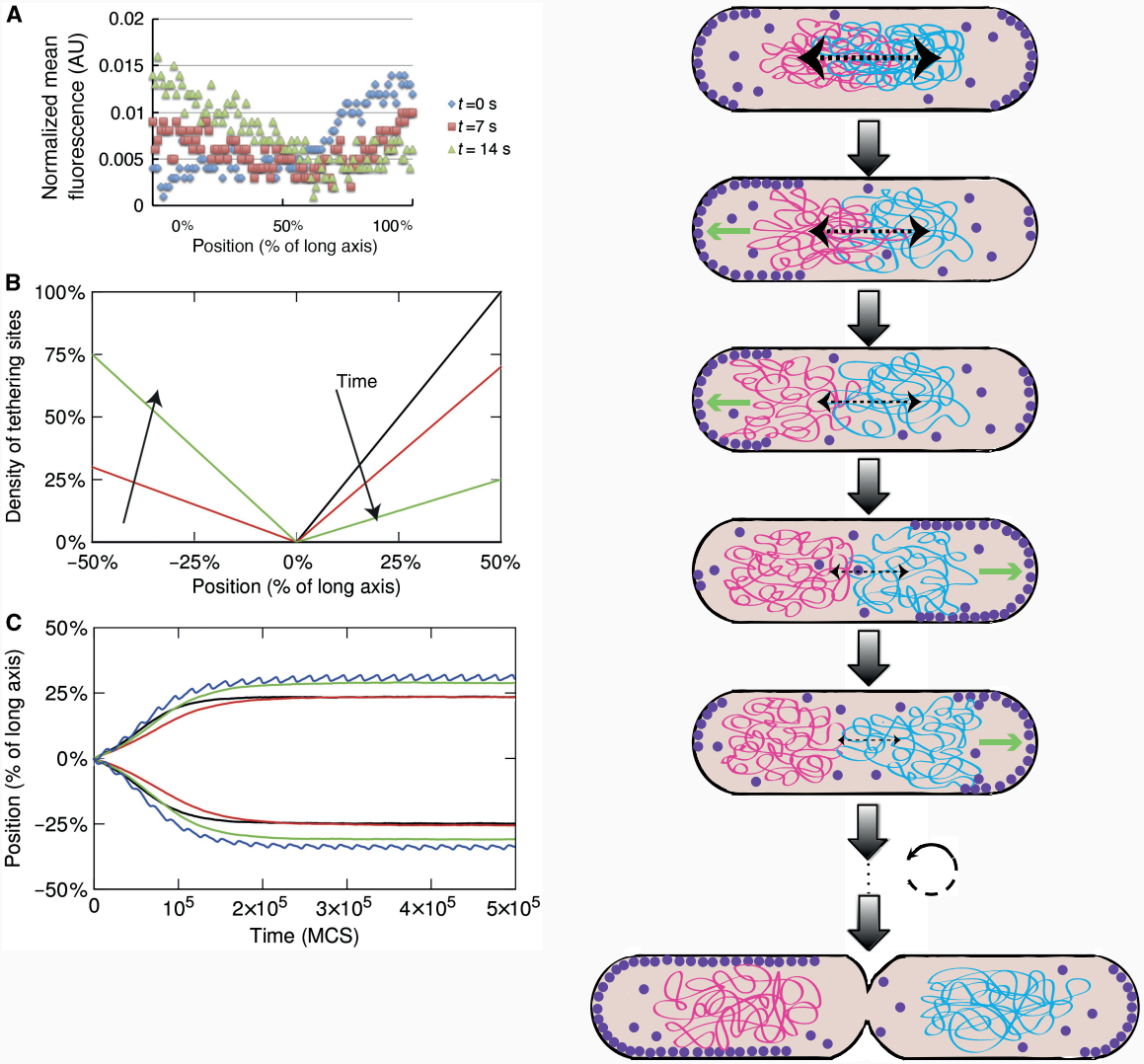

Figure 44: Disentangling of two circular chromosomes (cnt'd).

Membranes DNA Interaction VI

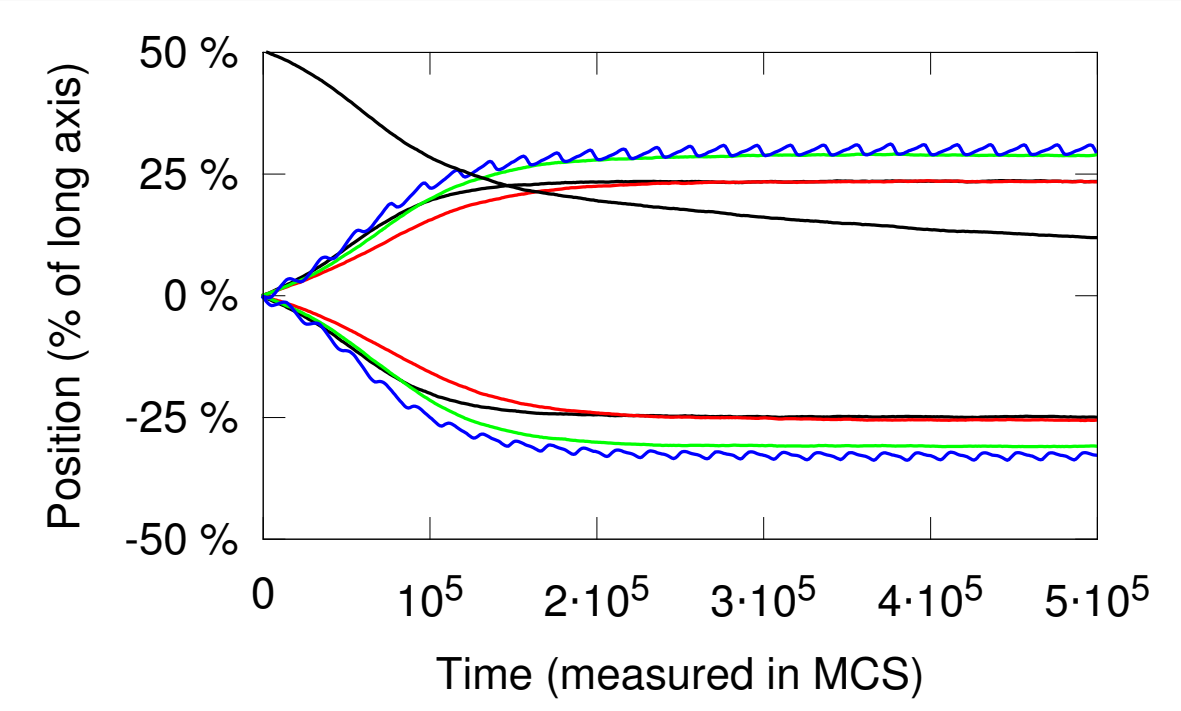

Figure 45: Disentangling of two circular chromosomes.

Excercises

Excercises I

Exercise 1: *tbd*

Bibliography

UNIVERSITÄT HEIDELBERG ZUKUNFT SEIT 1386

References

[1] T. J. Byers and D. Branton *Visualization of the protein associations in the erythrocyte membrane skeleton.* Proc. Natl. Acad. Sci. USA. 82:6153-6157. 1985.

[2] Felix Kapahnke, Ulrich Schmidt, Dieter W. Heermann, and Matthias Weiss. Polymer translocation through a nanopore: The effect of solvent conditions. *The Journal of Chemical Physics*, 132(16):164904, 2018/01/04 2010.

[3] Y. Kantor and 4020 D. Nelson, Phys.Rev. **A36**. For a review see *jerusalem winter school for theoretical physics: statistical mechanics of membranes and surfaces*, edited by d. 1987. Nelson, Piran.T., and S. Weinberg (World Scientific, 1989).

[4] F. Abraham and 2653 D. Nelson, J.Phys. France **51**. 1990. 1990.

[5] S. Chiruvolu M. S. Spector, E. Naranjo and **73** (21) 2867 J. A. Zasadzinski, Phys. Rev. Lett. 1994. 1994.

[6] D. Bensimon M. Mutz and **67** (7) 923 M. J. Brienne, Phys. Rev. Lett. 1991. 1991.

[7] 207 A. Polyakov, Physics Letters **103B**. 1981. 1981.

[8] J. Fendler and 3 P. Tundo, Acc.Chem.Res. **17**. 1984. 1984.

Bibliography II

[9] P. Bassereau F. Larche, J. Apell and 1700 J. Marignan, Phys.Rev.Lett. **56**. 1986. 1986.

[10] Y. Kantor and 2774 D. Nelson, Phys.Rev.Lett. **58**. 1987. 1987.

[11] B. Durhuus J. Ambjørn and 433 J. Fröhlich, Nucl.Phys. **B257**. 1985. 1985.

[12] 543 F. David, Nucl.Phys. **B257**. 1985. 1985.

[13] I. Kostov D. Boulatov, V. Kazakov and 641 A. Migdal, Nuclear Physics **B275**. 1986. 1986.

[14] R. Renken and 328 R. Kogut, Nuclear Physics **B354**. 1991. 1991.

[15] R. Renken and 554 J. Kogut, Nuclear Physics **B350**. 1991. 1991.

[16] R. Renken and 753 J. Kogut, Nuclear Physics **B342**. 1990. 1990.

[17] 209 T. Onogi, Physics Letters **B255**. 1991. 1991.

[18] R. Harnish and 861 J. Wheater, Nuclear Physics **B350**. 1991. 1991.

[19] D. Espriu M. Baig and 587 J. Wheater, Nuclear Physics **B314**. 1989. 1989.

[20] S. Catteral C. Baillie, R. Williams and 543 D. Johnston, Nuclear Physics **B348**. 1991. 1991.

[21] D. Johnston C. Baillie and 469 R. Williams, Nuclear Physics **B335**. 1990. 1990.

[22] 121 S. Catteral, Physics Letters **B243**. 1990. 1990.

Bibliography III

[23] 207 S. Catteral, Physics Letters **B220**. 1989. 1989.

[24] B. Durhuus J. Ambjørn and 526 T. Jonsson, Nuclear Physics **B316**. 1989. 1989.

[25] L. Peliti and 1690 S. Leibler, Phys.Rev.Lett. **54**. 1985. 1985.

[26] 1263 W. Helfrich, J.Physique **46**. 1985. 1985.

[27] 115 D. Förster, Physics Letters **114A**. 1986. 1986.

[28] 406 A. Polyakov, Nucl.Phys. **268B**. 1986. 1986.

[29] J. Ambjørn and 253 B. Durhuus, Phys.Lett. **B188**. 1987. 1987.

[30] B. Durhuus J. Ambjørn and 2619 T. Jonsson, Phys.Rev.Lett. **58**. 1987. 1987.

[31] J. Fröhlich J. Ambjørn, B. Durhuus and 480 T. Jonsson, Nuclear Physics **B290**. 1987. 1987.

[32] 271 D. Espriu, Physics Letters **194B**. 1987. 1987.

[33] R. B. Potts and C. Domb. Some generalized order-disorder transformations. *Proceedings of the Cambridge Philosophical Society*, 48:106, 1952.

[34] Ernst Ising. Beitrag zur theorie des ferromagnetismus. 31(1):253–258, 1925.

[35] C. Münkel and 2181 D. Heermann, J.Physique I **2**. 1992. 1992.

[36] D. Landau M. Challa and 37 K. Binder, J.Phys.II **1**. 1986. 1986.

[37] K. Binder and **30** (3) 1477 D. P. Landau, Phys. Rev. B. 1984. 1984.

Bibliography IV

[38] P. Peczak and 11932 D. Landau, Phys.Rev. **39B**. 1988. 1988.

[39] A. M. Ferrenberg and **63** (12) 1195 R. H. Swendsen, Phys. Rev. Lett. 1989. 1989.

[40] A. Ferrenberg and 2635 R. Swendsen, Phys.Rev.Let. **61**. 1988. 1988.

[41] J. Kogut S. Catteral, D. Eisenstein and 647 R. Renken, Nuclear Physics **B366**. 1991. 1991.

[42] R. Renken and 580 R. Kogut, Nuclear Physics **B348**. 1991. 1991.

[43] R. Renken and 580 R. Kogut, Nuclear Physics **B348**. M. 1991. Fisher, The theory of critical point singularities, in *Proceedings of the International School of Physics 'Enrico Fermi'*, 1971.

[44] F. F. Abraham and **252** 419 M. Kardar, Science. 1991. 1991.

[45] F. Abraham and 393 D. Nelson, Science **249**. 1990. 1990.

[46] J. Bouchaud and 2625 E. Bouchaud, Phys.Rev.Lett. **61**. 1988. 1988.

[47] S. Leibler E. Guitter, F. David and 2949 L. Peliti, Phys.Rev.Let. **61**. 1988. 1988.

[48] M. Kardar M. Paczuski and 2638 D. Nelson, Phys.Rev.Letters **60**. 1988. 1988.

[49] Y. Kantor and 4020 D. Nelson, Phys.Rev. **A36**. 1987.

[50] H. Lin S. Stupp, S. Son and L. Li. *Science*, 259:59, 1993.

[51] E. L. Thomas. *Science*, 259:43, 1993.

Bibliography V

[52] J. Flory. *Statistical Mechanics of Chain Molecules*. Interscience, 1969.

[53] D. Stauffer and A. Aharony. *Introduction to Percolation Theory*. Taylor and Francis, 2nd ed edition, 1992.

[54] K. Binder and D.W. Heermann. *Monte Carlo Simulation in Statistical Physics*. Springer-Verlag (first editon 1988), 2017.

[55] M. Kardar Y. Kantor and **57** 791 D. R. Nelson, Phys. Rev. Lett. 1986.

[56] C. Münkel and **3** 1359 D. W. Heermann, J. Physique I. 1993.

[57] M. Kardar and **38** 966 D. R. Nelson, Phys. Rev. A. 1988.

[58] W. E. Rudge F. F. Abraham and **62** (15) 1757 M. Plischke, Phys. Rev. Lett. 1989. 1989.

[59] J.-S. Ho and **63** 1324 A. Baumgärtner, Phys. Rev. Lett. 1989. 1989.

[60] M. Plischke and **38** 4943 D. Boal, Phys. Rev. A. 1988. 1988.

[61] B. J. Pendleton S. Duane, A. D. Kennedy and **195** (2) 216 D. Roweth, Phys. Let. B. V. 1987. Privman, *Finite Size Scaling and Numerical Simulation of Statistical Systems*, (World Scientific, Singapore, 1990).

[62] B. J. Pendleton S. Duane, A. D. Kennedy and **195** (2) 216 D. Roweth, Phys. Let. B. M. 1987. N. Barber, in *Phase Transitions and Critical Phenomena, Vol.8*, (Academic Press London, 1983).

Bibliography VI

[63] **43** 15 E. Brezin, J. Physique. 1982. 1982.

[64] M. E. Fisher and **28** (23) 1516 M. N. Barber, Phys. Rev. Lett. 1972. 1972.

[65] C. Borgs and **68** 1734 Kotecký, Phys. Rev. Lett. 1992. 1992.

[66] S. Kappler and **3** (5) 1099 C. Borgs, Int. J. of Mod. Phys. C. 1992. 1992.

[67] C. Borgs and **61** 79 Kotecký, J. Stat. Phys. 1990. 1990.

[68] J. Lee and **65** (2) 137 J. M. Kosterlitz, Phys. Rev. Lett. 1990. 1990.

[69] S. Grotehans and **41** (8) 4574 R. Lipowsky, Phys. Rev. A. 1990.

[70] Alwin Köhler and Ed Hurt. Exporting rna from the nucleus to the cytoplasm. *Nature Reviews Molecular Cell Biology*, 8(10):761–773, 2007.

[71] Suckjoon Jun and Bela Mulder. Entropy-driven spatial organization of highly confined polymers: Lessons for the bacterial chromosome. *Proceedings of the National Academy of Sciences*, 103(33):12388–12393, 08 2006.

UNIVERSITÄT
HEIDELBERG
ZUKUNFT
SEIT 1386

Index

Index I